INFORMATION TO USERS

This manuscript has been reproduced from the microfilm master. UMI films the text directly from the original or copy submitted. Thus, some thesis and dissertation copies are in typewriter face, while others may be from any type of computer printer.

The quality of this reproduction is dependent upon the quality of the copy submitted. Broken or indistinct print, colored or poor quality illustrations and photographs, print bleedthrough, substandard margins, and improper alignment can adversely affect reproduction.

In the unlikely event that the author did not send UMI a complete manuscript and there are missing pages, these will be noted. Also, if unauthorized copyright material had to be removed, a note will indicate the deletion.

Oversize materials (e.g., maps, drawings, charts) are reproduced by sectioning the original, beginning at the upper left-hand corner and continuing from left to right in equal sections with small overlaps.

Photographs included in the original manuscript have been reproduced xerographically in this copy. Higher quality 6" x 9" black and white photographic prints are available for any photographs or illustrations appearing in this copy for an additional charge. Contact UMI directly to order.

Bell & Howell Information and Learning
300 North Zeeb Road, Ann Arbor, MI 48106-1346 USA
800-521-0600

UMI®

Modelling the interannual variability of the Arctic sea ice cover

by

Gilles Arfeuille

Department of Atmospheric and Oceanic Sciences
and the
Centre for Climate and Global Change Research
McGill University, Montreal, Quebec.

Submitted to the Faculty of Graduate Studies and Research in partial fulfillment of the requirements for the degree of Master of Science.
November, 1998

Abstract

A thermodynamic-dynamic sea ice model based on the granular material rheology of Tremblay and Mysak is used to study the interannual variability of the Arctic sea ice cover during the 41-year period 1958-1998. The sea ice model is coupled to both a mixed layer ocean model and a one-layer thermodynamic atmospheric model. The model is first run with monthly climatology for most of the thermodynamic and dynamic forcing components (air temperature, ocean temperature, wind stress) to obtain a stable periodic seasonal cycle (the ocean currents are set at their annual mean values). For the 41-year run, the monthly wind stress forcing is derived from analyzed sea level pressures from the National Centers for Environmental Prediction (NCEP Reanalysis) data. The atmospheric thermodynamic forcings are based on monthly climatology.

In this thesis we explore the high-latitude sea ice circulation and thickness changes due to year-to-year variations in the wind field. We focus our study on the interannual variability of the sea ice volume in the Arctic Basin, and the subsequent changes in the export of sea ice from the Arctic Basin into the northern North Atlantic via Fram Strait. The latter quantity is an important input of fresh water into the North Atlantic and can be the origin of important ocean climate events like the Great Ice and Salinity Anomaly of the 1960s/1970s. Therefore, we first examine in detail the time series of Fram Strait sea ice export for the 41-year period 1958-1998. The model results are compared with other sea ice export simulations covering the 1960-1985 period, and with sea ice export data measured during the 1990-1996 period. The comparative role of the sea ice thickness and velocity in the sea ice export anomalies are especially investigated, and the former is shown to be particularly important. The sea ice export anomalies are next related to the prior sea ice volume anomalies in the Arctic Basin. Finally, the origin and evolution of the latter anomalies are related to the sea ice circulation and atmospheric forcing patterns. It is shown that large sea ice export anomalies are generally preceded by large volume anomalies formed along the

East Siberian Coast due to anomalous winds. The latter happen when the Beaufort High is centered closer than usual to this region. When the Beaufort High relocates near the Beaufort Sea and the Icelandic Low extends far into the Arctic Basin, the ice volume anomalies are transported to the Fram Strait region via the Transpolar Drift Stream.

Finally, the sea ice export through Fram strait is compared with the North Atlantic Oscillation (NAO) index. A high correlation between the two quantities is not evident for the full duration of the study. Thus, this suggests that the Arctic Basin should be considered as a particular region in order to understand the influence of the atmospheric conditions on the sea ice cover there.

Résumé

Dans la présente thèse, nous utilisons un modèle thermodynamique et dynamique de glace de mer pour étudier la variabilité inter-annuelle de la couverture de glace dans l'Arctique, ceci pour une période de 41 années allant de 1958 á 1998. Le modèle de glace de mer utilisé ici est basé sur une rhéologie de type granulaire développée par Tremblay et Mysak. Ce modèle est couplé à un modèle simple d'océan (couche de mélange uniquement) et aussi à un modèle thermodynamique d'atmosphère à une couche. Avant d'éffectuer la simulation principale, l'état d'équilibre pour le modèle océan-glace-atmosphère est atteint à l'aide d'une simulation d'une durée de 20 ans utilisant la climatologie des 41 années des données "NCEP Reanalysis". Une autre simulation est alors effectuée à l'aide des données NMC pour la période 1954-57 pour débuter la simulation de 41 ans avec de meilleures conditions initiales. Cette dernière simulation est accomplie en utilisant les moyennes mensuelles des stress dûs aux vents et les moyennes climatologiques pour les autres entrées.

Le but majeur de cette thèse est d'étudier les changements de la circulation et de l'épaisseur de la glace de mer dûes aux variations d'année en année des vents en hautes latitudes. La variation inter-annuelle des volumes de glace de mer dans le bassin Artique et celle des exports subséquents de glace vers l'Atlantique Nord à travers le détroit de Fram sont tout particulièrement étudiées.

Dans le but de valider les anomalies de l'export de glace de mer à travers le détroit de Fram, des comparaisons sont effectuées entre les valeurs de ces anomalies et celles obtenues à partir d'autres simulations pour la periode 1960-85 et aussi avec des observations effectuées pendant la période 1990-96.

Ceci fait, en décomposant la valeur des anomalies d'export en anomalies d'epaisseur et de vitesse, l'importance de l'épaisseur de glace dans l'export est démontrée. L'importance de cette glace de mer particulièrement épaisse et formée dans le bassin Arctique, nous amène à considérer les importantes anomalies de volume formées dans ce bassin, précédant et causant chaque important export de glace

de mer à travers le détroit de Fram.

L'origine et l'évolution de ces anomalies de volumes sont finalement reliées à la circulation de la glace dans le bassin Arctique et à la situation atmosphérique causant cette circulation. Il est démontré que chaque période comprenant un important export de glace de mer est précedée par une période d'augmentation de volume dans le bassin d'une valeur comparable à l'export. Cette augmentation de volume est dûe à de la glace épaisse généralement formée le long de la côte Est siberienne. Cette formation de glace épaisse est dûe à des conditions non-habituelles de vents. Ceci arrive quand l'anticyclone de la mer de Beaufort est centré plus proche de cette région que d'habitude. Ce n'est que quand cet anticyclone se recentre prés de la mer de Beaufort et que la dépression d'Islande s'étend loin dans le bassin Arctique, que les anomalies de volumes sont transportées à travers le bassin via le courant de dérive transpolaire vers la région du détroit de Fram.

Finalement, la variation des anomalies de l'export de glace de mer à travers le détroit de Fram est comparée à l'indice NAO. Une correlation inportante n'est pas évidente pour la période de 41 ans et ceci suggère que le bassin Arctique devrait être considéré comme une région particulière dans le but ultime de comprendre l'influence des conditions atmosphériques sur la couverture de glace de mer en hautes latitudes.

Remerciements

Mes remerciements vont tout d'abord à mon directeur de thèse, le professeur Lawrence A. Mysak, qui a démontré une confiance constante dans mes travaux. Il m'a toujours donné de très bons conseils et tous les moyens disponibles pour effectuer ma recherche en me laissant une grande liberté, me responsabilisant et m'impliquant ainsi le plus possible. Il a aussi été très patient avec mon anglais, et je le remercie d'avoir vérifié avec grand soin le présent manuscrit.

Mes remerciements vont aussi tout spécialement au Docteur Louis Bruno Tremblay, concepteur du modèle utilisé dans cette thèse et qui a toujours répondu à mes très nombreux courriers électroniques journaliers et a toujours été de bon conseil.

Je tiens à remercier mes collégues toujours présents et enthousiastes pour répondre à mes avalanches de questions, je pense ici entre autres à Zhaomin Wang pour sa patience et ses conseils pour la programmation en langage Fortran, au Docteur Halldór Björnsson véritable source de science toujours vaillant pour de bonnes discussions scientifiques. Je pense aussi à Natalie Hasell qui n'a jamais hésité à consacrer du temps pour corriger mon anglais dans mes écrits. Elle a ainsi participé grandement à l'amélioration de mon anglais. Mes remerciements s'adressent aussi à tous les autres qui oeuvrent dans le département de sciences atmosphériques et océaniques, en n'oubliant surtout pas les personnes de l'administration du département qui font de celui-ci un lieu si particulièrement accueillant et propice au travail de recherche.

Ce travail a été financé grâce aux subventions de recherches accordées au professeur Lawrence A. Mysak par les fonds de recherche NSERC et FCAR. Le salaire pour mon premier été de recherche, accordé par le Centre de Recherche sur le Climat et les Changements à l'Echelle du Globe (C^2GCR), a été grandement apprécié.

Je tiens à remercier en dernier lieu tous ceux que j'ai croisé ou que je croiserai sur mon chemin, je pense ici à Normand, Sylvie, Geneviève ,Béatrice, Bruce, Jacques, Daniel, Kerry, Luc, Bekkha et tous les autres.

Contents

List of Tables

List of Figures

Chapter 1

Introduction

Large-scale atmosphere-ocean interactions have a strong influence on weather and climate variability. Therefore, knowledge and understanding of the type and evolution of these interactions are very important. In some polar regions, the ocean and surrounding seas are covered permanently and seasonally in others by the constantly evolving pack ice, which significantly affects these interactions. Sea ice covers 7% of the earth's oceans, and thus represents a non-negligible part of the air-ocean interface. Sea ice has a strong influence on polar climate in particular and global climate in general, because it reflects a large part of the incoming solar radiation and restricts exchanges of heat, moisture and momentum between the ocean and the atmosphere.

By acting as an insulating blanket over the relatively warm ocean, Arctic sea ice substantially influences the atmospheric energy budget. The latter is highly dependent on heat released during the freezing of water and absorbed during the melting of ice at high latitudes. In this way, sea ice has strong effects on the dynamics and thermodynamics of the ocean and atmosphere. The latter components of the climate system also feed back to sea ice. The ocean provides currents and heat transfer forcing, and the atmosphere produces heat transfer, precipitation and wind forcing. Both play an important role in determining sea ice variability. The major determinants of the dynamic and thermodynamic variability of the sea ice in the Arctic are atmospheric fields of wind and temperature (Tremblay and Mysak, 1998). Because of the

high sensitivity of sea ice cover to atmospheric changes, this medium can be a good indicator of climate change associated with global warming, expected to be amplified in the polar regions. This makes it very important, therefore, to understand the dynamics and the thermodynamics of sea ice natural variability, in order to separate it out from anthropogenically forced changes.

Interest in Arctic climate variability has also been motivated by notable ocean climate events at high latitudes such as the Great Salinity Anomaly (GSA) (or Great Ice and Salinity Anomaly (GISA)). This was an advective feature in the northern North Atlantic consisting of upper ocean negative temperature and salinity anomalies in the late 1960's and 1970's. Dickson *et al.* (1988) claimed that it was "the most persistent and extreme variation in global ocean climate yet observed in this century." The GSA was accompanied by large sea ice extents in the Greenland Sea and then in the Labrador Sea (Mysak and Manak, 1989, Mysak *et al.*, 1990); the peak in the Greenland Sea occurred in 1968 (Walsh and Johnson, 1979). Because of the association of the GSA with the ice anomalies, Mysak and Power (1992) renamed the GSA as the GISA.

It appears that the GISA affected the thermohaline circulation and the deep water formation in certain parts of the northern North Atlantic (Lazier, 1980). The deep water formation in the Greenland, Norwegian, Iceland and Labrador seas is considered to be the main driving force of the global ocean thermohaline circulation, the so-called global conveyor belt, and the formation rates depend on the surface water salinity and temperature. When salinity is large and cooling is substantial, the surface water is so dense that the water column becomes statically unstable and deep water formation (convection) occurs. Aagaard and Carmack (1989) noted that presently the northern North Atlantic region does not require dramatic increases in the fresh water flux from the Arctic to effect a capping of convection. In the Greenland, Iceland, and Norwegian seas (GIN Sea) and the Labrador Sea, the main source of fresh water is sea ice. Ice floes can be advected from the Arctic Ocean by winds and ocean currents following the Transpolar Drift Stream and the East Greenland Current (Häkkinen,

1993). Therefore sea ice export from the Arctic ocean to these regions through Fram Strait can have a strong influence on deep water formation in the Greenland and the Iceland Seas. Recently, Anderson *et al.* (1998) have questioned the northern hemisphere origins of the dense water that drives the conveyor belt. They argued that, since deep convection in the Greenland Sea and the Iceland Sea has seasonal and decadal variability, dense water flowing over the Greenland-Scotland Ridge into the North Atlantic should have the same seasonal and decadal variability. But since the latter has remained remarkably constant over the recent years, they think that this dense water should have another origin than deep water formation in the GIN Sea. They argued that this dense water could be formed from deep convection processes in the Arctic Ocean, especially over the shelves during ice formation. This issue adds to our motivation to improve our knowledge and understanding of the changes in the ice conditions in the Arctic and in the mechanisms for these changes.

During the past few decades, several studies have been published on the seasonal and interannual variability of sea ice cover in the Arctic, and to a lesser extent, in the Antarctic. Some are numerical modelling studies, while others are statistical (data based) investigations. The latter, using reconnaissance flight and ship observations, station data, submarine upward-looking sonar data or satellite passive-microwave data, show the extent and nature of these fluctuations. Parkinson and Cavalieri (1989) pointed out that "passive-microwave data confirm that the sea ice covers of the northern and southern hemispheres exhibit very strong seasonal cycles and considerable interannual variability." Satellite data give a very good estimate of sea ice extent, but these are only available since the early 1970's. Arctic buoy experiments give quantitative estimates of the mean sea ice velocity field. But, since the Arctic and Antarctic regions are difficult to access, taking extensive measurements to estimate the sea ice thickness distribution is not possible. Thus modelling studies play an important role in understanding sea ice behavior. Some important modelling work has been done during the last three decades to understand the role of different types of forcing in producing the sea ice variability.

In the present study, the main objective is to better understand mechanisms involved in producing the interannual sea ice cover changes in the Arctic with emphasis on the role of the atmospheric wind forcing. To achieve this objective we integrate a thermodynamic-dynamic sea ice model based on granular rheology (Tremblay and Mysak, 1997) for the last 41 years, from January 1958 to June 1998. To determine which interannual changes in Arctic sea ice cover are due to changes in the wind field, only monthly mean wind stresses are varied from year to year, while all the other atmospheric and oceanic forcings are set to climatological values.

After a review of some important modelling studies relating interannual sea ice cover to various forcing effects (chapter 2), the model and the domain used in this thesis are presented in chapter 3. In chapter 4 data used for the simulations as well as the experiments run are described. In order to analyze the results of the 41-year run, the Fram Strait sea ice export results are compared with model results from another study for the 1960-85 period in chapter 5. The results are then compared with sea ice export data measured in the Fram Strait region during the 1990-1996 period. Next we examine the interannual variability of the sea ice export through Fram Strait, with a particular focus on the roles played by the sea ice thickness and velocity in the year-to-year variations. The relation between the sea ice export through Fram Strait and the origin of important climatic events like the aforementioned GISA of the 1960's/1970's This outflow is then related to events in the Arctic basin itself, especially to sea ice volume anomalies in the Arctic basin. Finally, the origin of these sea ice volume anomalies and their propagation in the Arctic Basin are described and related to the atmospheric forcing field. A summary of the results is given in chapter 6.

Chapter 2

Literature Review

Important modelling work has been done during the last three decades to understand the role of different types of forcing in producing sea ice cover variability.
In 1960's and early 1970's, numerical models were either of a dynamic or thermodynamic type. In these first studies, investigators considered ice to be a highly viscous Newtonian fluid, and models were developed taking into account parameterization of the interactions between ice floes. With this as a background, Campbell (1965) proposed the first dynamic model for ice drift in the Arctic. At the same time, thermodynamic models for sea ice were also being developed; an elaborate model is the one-dimensional thermodynamic model of Untersteiner (1961) which described sea ice seasonal growth and ablation. The model was refined a decade later to include snow cover (Maykut and Untersteiner, 1971). The vertical resolution of this model is so fine, however, that its application to large regions such as the entire Arctic is impossible because the computationnnal cost would be too high. Also, this aspect inhibits its extension to a three-dimensional framework. Therefore, Semtner (1976a) developed a simplified version of the Maykut and Untersteiner model for use in climate studies. The Semtner model consists of one layer of snow and three layers of ice (and can be extended to n layers), with a 30-m oceanic mixed layer beneath the ice.

During the same period, Semtner (1976b) developed an ocean model for the Arctic. This was the first three-dimensional simulation of the circulation at northern high

latitudes. This general circulation ocean model has 14 vertical levels. To drive the ocean, an indirect method was used. Since only the major features of ice drift were known at the time, Semtner assumed that long-term forcing of the wind on sea ice was transmitted to the water beneath the ice with little modification. Long-term averages of atmospheric pressure were used to compute the wind stress, which was assumed to act directly on the ocean, and was computed using a quadratic drag law with a large drag coefficient. However, it is now known that, in the Arctic, momentum is transmitted to the ocean primarily by the motion of the overlying sea ice.

Later, after improvements to the different types of ice models, the dynamics and thermodynamics of sea ice were combined into one model and used for longer timescale runs. It was then possible to investigate the relative effects of thermodynamics and dynamics on the seasonal and interannual sea ice changes in the polar oceans. Parkinson and Washington (1979) developed a large-scale sea ice model, which included four layers (ice, snow, ocean, atmosphere); however, ice motion was not coupled to the ocean circulation, a prescribed feature.

Hibler (1979) developed a sea ice rheology relating ice deformation and thickness to internal stresses in the ice cover using a viscous-plastic rheology, which considers the ice to behave as a non-linear viscous compressible fluid. His main goal was to study the Arctic sea ice cover emphasizing the effects of ice dynamics on ice thickness distribution and vertical heat flux. In this dynamic-thermodynamic sea ice model, a two-level approximation is made for the ice cover, consisting of thin or thick ice. Thin ice is characterized by a certain areal fraction of open water, while thick ice, covering the remaining area, is taken to be of constant thickness. The thermodynamic part of the model is introduced by the addition of sink and source terms in the continuity equations, which represent the effects of growth and decay of the thickness distribution.

After these pioneering studies, other important investigations were conducted to understand the role of the thermodynamics and dynamics in the temporal and spatial variability of sea ice cover. Some studies focused on the importance and effects of

the dynamic and thermodynamic parts of the sea ice model itself, while others dealt with the ocean component.

2.1 Hibler and Walsh (1982)

The first step toward a quantitative model-based examination of the role of atmospheric forcing in producing interannual variability of Arctic sea ice was presented in Hibler and Walsh (1982). They extended the dynamic-thermodynamic model of Hibler (1979) to include not only the Arctic basin but also the peripheral seas and the marginal ice zone. They performed simulations using observed daily atmospheric forcing fields for the three-year period, 1st January 1973 to 31st December 1975. Their goals were to determine (1) the degree to which the model could simulate seasonal and interannual fluctuations, and (2) the part of the model that needed improvement.

The dynamic part of the model used is the same as in Hibler (1979). The thermodynamic portion is a simplified version of Semtner (1976a). Thermodynamic computations were performed for two levels (open water, h=0, and an average thickness over the rest of the grid cell). The snow cover was parameterized only through the surface albedo which takes the value of ice albedo for temperatures above the freezing point and the value of snow albedo below the freezing point. The sea ice growth rate was calculated using Semtner's model with a motionless oceanic mixed layer.

Data sets of sea level pressure from the National Center for Atmospheric Research (NCAR) were used to compute the daily geostrophic wind field which drives the model. Surface air temperature and relative humidity fields were taken from the National Meteorological Center (NMC).

Two types of simulation were done, one using the thermodynamic part alone and the other using the complete model. The simulations in both cases yielded a seasonal cycle with excessive amounts of ice in the North Atlantic during winter and excessive amounts of open water in the central Arctic during summer. Despite these seasonal biases, the simulated and observed interannual fluctuations were similar in

magnitude and positively correlated. This was especially true in the case of the complete dynamic-thermodynamic model results.

The model results showed light summertime ice conditions for the year 1973 and heavy ice conditions for the year 1975. The observed interannual differences (Barnett, 1980) indicated that along the Alaskan coast 1973 was the fifth lightest year of ice cover. 1974 the tenth lightest and 1975 the most severe of the 23 summers from the 1953-75 period. There was also good agreement between the simulated and observed August ice edge of 1974 in the Kara Sea.

To obtain an overall quantitative examination of the interannual fluctuations, data and the model results were compared both for the ice covered area (equal to the sum of products of compactness and grid cell area) and for the area within the ice edge where the ice edge was defined by grid cells with compactness equal to 10%. The time series of the simulated and observed fluctuations of the ice edge and the ice covered area were computed in a 30° longitudinal sector (20°W-10°E) covering the East Greenland Sea region. The correlation was higher for the ice edge fluctuations (0.58 for the complete model, 0.64 without dynamics) than for the ice covered area (0.40 for the complete model). Even though the results were positively correlated, due to the seasonal bias, the simulated fluctuations represented a smaller percentage of the annual cycle than were observed.

Another important quantity is the ice outflow from the Arctic basin into the eastern part of the Greenland Sea via Fram Strait since this has a significant impact on the regional sea ice mass balance. The transport of latent heat of fusion with this ice outflow is the second component of the advective heat budget of the Arctic Ocean after the warm Atlantic layer entering the Arctic (Aagaard and Greisman, 1975). Values of the monthly ice mass outflow, during 1973-75 were computed across 80°N through Fram Strait. The monthly differences in sea level pressure Δp, between (80°N,20°W) and (80°N,20°E), and the outflow show a correlation of 0.91, 0.34 and 0.22 at ice outflow lags of 0, 1 and 2 months respectively. Since Δp measures the northerly component of the monthly geostrophic wind in Fram Strait, the correlations

indicate that the fluctuations of ice outflow can be viewed as rapid responses to wind fluctuations on monthly to seasonal time scales. A particularly interesting feature of the ice export from the Arctic is that this quantity has a strong interannual variability. The latter is also true for the wind field. The total outflow during 1974 was approximately half as large as that during 1973 and during 1975. The year-to-year variations of the annual ice export are quite important. These are very consistent with the variations in heat and water fluxes in the Fram Strait region estimated by Aagaard and Greisman (1975). An important factor affecting the interannual variation of the sea ice export could be the heat transported northward by the West Spitsbergen current. They estimated that the interannual variability of the relatively warm Spitsbergen current contributes to 35% of the variations of the seasonnal influx of water.

2.2 Walsh, Hibler and Ross (1985)

Since the preceding three-year study was too short to permit the compilation of reliable statistics, Walsh *et al.* (1985) extended the earlier simulations to a decadal scale and expanded the domain to include a large portion of the sub-arctic Pacific. The domain was divided into 18 different sectors. Alternative sets of forcing data were used to test the sensitivity of the model to the origin of atmospheric forcing data. The dynamics of the ice model was the same as before, but several changes in the thermodynamics were made.

Snow cover was now explicitly represented. Ice thickness and snow cover are partitioned into a seven-level distribution. Snow was accumulated during the non-summer months using prescribed accumulation rates (Parkinson and Washington, 1979). The presence of brine pockets and the penetration of solar radiation were neglected. This resulted in a too rapid summer melt over too large an area, giving a distorted simulated seasonal cycle. Observed atmospheric forcing data were used to run the model with a one-day time step for the 30-year period 1951-1980. Geostrophic

daily wind fields were computed from NCAR sea level pressure analyses. Two different sources were used to obtain the daily temperature fields by adding the temperature anomalies from the Russian (20 years of available data) and NASA (30 years) data sets to the climatological means.

The major objectives of their work were to analyze large-scale multi-year sea ice fluctuations in terms of ice mass budgets and to determine the relative roles of dynamic and thermodynamic processes in producing interannual variability of sea ice cover. To examine the latter, different simulations were performed with and without dynamics, and with two different sets of atmospheric temperature forcing fields. One temperature field was obtained from the NASA Goddard Institute, the second one from Russia (Vinnikov, 1977). Comparisons of these results with observations helped the authors chose which set gave the most valid simulated interannual variations. Since the NASA-derived results showed better correspondence with observations and were available for 30 years, the observational comparison and the mass budget analysis were based on simulations using the NASA 30-year data sets.

The results showed that the interannual fluctuations as well as the mean fields are more realistic when the model includes dynamics. A good illustration of the interannual variations was the ice edge position at the end of August during 1968 and 1975. These were respectively the lightest and heaviest ice summers in the Alaskan Arctic region during the 1953-1977 period. The simulated ice edge in 1968 was farther poleward than observed, but the nearshore position in 1975 agreed well with that observed. Both of the model results and observational data showed that similar extremes were not observed in the European Arctic region, where the ice extent was greater in 1968 than in 1975.

The authors also noticed longer-term (decadal-scale) changes in the ice drift patterns. The pattern of the Arctic Ocean anticyclonic gyre and the Transpolar Drift Stream slowly changed, keeping roughly the same state during five-year periods.

The sea ice mass budgets calculated from the fields of ice thickness, growth, and velocity provided by the simulations showed generally good agreement with available

observational data in the Arctic basin. In the annual cycle, the thermodynamic processes appear to be dominant but advective processes made relatively important contributions to interannual fluctuations of ice mass.

The annual export of ice out of the Arctic through Fram Strait or, in some seasons, through Bering Strait showed strong interannual excursions. During the 30-year period studied (1951-80), the annual outflow through each strait often varied by a factor of 2 or 3 in successive years. For Bering Strait, the ice mass outflow varied from 1.36×10^{-2} (in 1974) to $-10^{-4} Sv$ (in 1967). The outflow for the Fram Strait is larger by one or two orders of magnitude. The smallest annual outflows occurred in 1963 and 1964, which were followed by a steady increase in the outflow. This steady increase led to a weak but positive linear trend in the 30-year time series of outflow amounts.

In the central Arctic, the correlation between ice transport variability and geostrophic wind fluctuations was found to be typically 0.8 or 0.9; in Fram Strait this quantity is only around 0.55. Here effects of the temporal variability of the ocean currents on sea ice variability could be important. Inclusion in the model of these effects can also remove the excessive winter ice extent in the northern North Atlantic.

2.3 Fleming and Semtner (1991)

To examine the importance of interannually varying ocean forcing on sea ice cover variability in the Arctic, Fleming and Semtner (1991) used a fully prognostic coupled ice-ocean model. Simulations were conducted for the 10-year period from January 1971 to December 1980 in which the coupled ice-ocean model was forced by a prescribed interannually varying atmosphere.

In this study, the authors used the Semtner model (1987) with some modifications. The domain included the Norwegian and Greenland seas and the entire Arctic basin. Since regional variations are significant, the domain was divided into four regions to gain an appreciation of these differences. The ocean model was composed of 13 fixed

layers and included bottom topography. This model was coupled with the ice model by momentum, heat, and salt exchanges through the ocean mixed layer, which was assumed to be completely mixed and was a constant 30 meters in thickness.

The data fields for the interannually varying atmospheric forcing were provided by Walsh and consisted of monthly compiled averages of observed surface pressure, specific humidity, longwave and shortwave radiation and air temperature. Monthly values of the major river inflows were specified. Boundary conditions for inflow and outflow were also specified and were invariant in time.

To determine whether interannual changes in ocean forcing affected sea ice, two different types of simulation were done using the same atmospheric forcing. Both were for a 10-year period, chosen for the accuracy of the observed ice concentration data set during this period. Simulation I was performed with the complete coupled ice-ocean model (interactive ocean model), and simulation II used a specified 10-year mean ocean circulation and ocean heat flux (with an annual cycle) computed from the first simulation (in which the ocean forcing is a prescribed mean annual cycle). The two sets of results were compared with observed data.

In both cases, the ice edge was reasonably well reproduced, particularly from December to May when ice was being formed, but there was insufficient ice cover in summer. The ice edges for the various years from simulation I were usually closer to the observed ice edges than those of simulation II. Even though the ice edge position was quite similar in both cases, there were large differences in thickness distribution and thickness variability. In ice compression regions along the north coast of Greenland and the Canadian Archipelago, simulation I thicknesses tended to be larger than those for simulation II, and in better agreement with observations.

Comparisons between the observed and calculated ice edges and oceanic heat flux contours produced by simulation I demonstrated a strong degree of interannual variability. The ocean heat flux appeared to produce noticeable changes in the position of the ice edge. The vertical component of the ocean heat flux (positive upward) seemed to be the dominant component controlling changes to the annual cycle of total ice

area and the interannual variations. Where ice cover was normally found throughout the year (*i.e.*, in the central Arctic), this flux was about 5 Wm^{-2}. Near the coastlines, this flux remained positive and had a strong annual cycle. Near the ice edge however, this flux varied from 180 Wm^{-2} in winter to -200 Wm^{-2} in summer. Influenced by the ocean heat flux, the simulated ice thickness contours displayed significant interannual variations; this provided an indication of how the ice within the pack responds to interannual variations of the forcing.

The monthly mean currents varied in both position and strength. Interannual variations of up to 25% were regularly observed in the Barents and Norwegian seas and over the Arctic shelves. The major gyres in the central Arctic basin were less variable. Except for the Transpolar Drift Stream and the East Greenland Current, variations in ocean currents appeared to be of secondary importance in influencing the location of the ice edge and the ice concentration.

The absolute value of the difference between the simulated and observed ice area can be used to determine how the simulated field differs. This quantity, for simulation I, was consistently less than the value for the second simulation, particularly in the GIN sea, which pointed to the more realistic results given by the interactive ocean model. To produce the anomaly data sets, the authors removed the mean annual cycle of the ice cover from the observed data and from both of the simulation results. From this, anomaly times series were analyzed. The ability of the simulated anomaly series to reproduce the observed series tests the robustness of the model to properly simulate the interannual variability.

The time series of ice area anomalies were computed for each of the four regions and showed considerable differences, indicating that the large scale ice area anomalies are localized features. Since the thermodynamic atmospheric forcing in this model has a relatively uniform annual cycle across all four regions, the ocean heat flux is the dominant mechanism controlling these localized changes. Furthermore, correlations between the model ice area fluctuations and the observed fluctuations were consistently higher for simulation I using an interannual ocean forcing than for simulation

II using a prescribed mean annual cycle ocean forcing as described above.

2.4 Häkkinen (1993, 1995)

Using a fully prognostic coupled Arctic ice-ocean model, Häkkinen performed two different studies on interannual variability, one specifically on sea ice (Häkkinen, 1993), and the second on deep water formation in the Greenland Sea gyre (Häkkinen, 1995). The model was composed of a thermodynamic part adapted from the Semtner (1976a) model with some modifications to account for ice leads. The dynamic part of the ice model was described as a continuum with a generalized viscous rheology but with a maximum pressure which has a quadratic dependence on ice thickness. The resulting dynamic-thermodynamic model was coupled to an ocean model via interfacial stresses and via salinity and heat fluxes through the ice-water interface. The ocean model was hydrostatic and Boussinesq. The equation of state is formulated in terms of *in situ* density which was expressed in terms of potential temperature, salinity and pressure. The ocean model used a sigma-coordinate system, and was composed of 18 levels.

The same data sources were used to force the model in both of these studies. In order to separate the influence of the wind forcing, in the atmospheric forcing, only the wind fields varied interannually. The transport (inflow/outflow) at lateral oceanic boundaries was prescribed and river runoffs were specified from the annual hydrographic climatology of Levitus (1982). Atmospheric forcing fields were composed of monthly climatological air temperatures (from Crutcher and Meserve (1970)) and daily geostrophic winds computed from the NCAR sea level pressure data sets. Finally, the monthly cloudiness and snow fall were assumed to be spatially constant and were taken from Huschke (1969) and Maykut and Untersteiner (1971).

The purpose of the 1993 study was to examine the interannual variability of sea ice during the 1955-1975 period , which included the GSA (or GISA) event. It was hypothesised that the GSA was a consequence of the anomalously large ice export in 1968, due to prior wind field changes in the Arctic Basin.

The results show that the largest variability in sea ice thickness takes place in the coastal regions, where winds can pack ice against the coast in winter, and where ice is less compacted and more free to move in summer. The least variability occurs in the central pack, especially in the Beaufort Gyre.

In the simulations, large Greenland ice extents were always preceded by large pulses in Fram Strait ice export. The largest simulated ice export was in 1968, about twice as large as the average, and it corresponded to the largest observed ice export. The changes in the transport pattern in the Arctic were responsible for the increase in ice export, namely the widening and strengthening of the Transpolar Drift Stream that covered most of the central basin and funnels ice to Fram Strait. Analysis of the annual averages of the forcing pressure fields revealed the long absence of the Beaufort High during the mid-1960's. The return of a strong anticyclone in 1968 coincided with the largest simulated ice export, and also the Transpolar Drift Stream became wider. To intensify the latter, a well-developed low pressure system extending from the Iceland Sea to the Barents and Kara seas seemed to be required. Both of these high and low pressure areas contributed to drive the ice velocities and ice cover anomalies and thus advect thicker ice into the subpolar gyre region of the North Atlantic.

In the late 1960's, freshwater excess in the Greenland Sea was so large that there must have also been some liquid freshwater exported from the main Arctic Basin. The variability in the modelled ice production or melt characterized by the surface salinity flux produced strong salinity anomalies, which were transported by the currents anticyclonically (clockwise) around the main Arctic Basin. The sharp increase in ice mass after 1972 was due to mechanical pile-up in the Canadian Basin and to a decrease in ice export. This anomaly along the Alaskan and Canadian coasts could have created an ice production deficit and a strong freshening. The results showed that this could have been be accomplished by a strong Siberian High. The increase in the Greenland sea ice cover coincided with the arrival of these fresh salinity anomalies. Therefore, the latter could have initiated or amplified the large ice extent anomalies.

Häkkinen (1995) focused her work on the interannual variability of deep water formation in the Greenland Sea gyre between 1955 and 1985 by investigating the variability of the gyre temperatures and salinities and relating the variability to surface forcing (wind stress, wind stress curl, and the heat and salinity fluxes).

The heat content of the upper 2000-m water column showed considerable variations during the 1960-1985 period. But the warming and cooling periods were not simultaneous with the salinization and freshening periods. Deep convection in the Greenland Gyre seems to have taken place during 1967-1969 and 1975-76, the coolest periods. Since the upper water column was much cooler than the seasonal average, the water column became unstable in winter. After 1978 the modelled column was stable and thus extensive deep water production was not expected. The results clearly show salinization and freshening periods for the upper water column. Consistent with the observations, the strongest modelled freshening period in the end of the 1960s corresponded to the GISA period. Another freshening event took place in 1984, and the ice export from the Arctic was considerably higher during the 1981-83 period. This was not the case for the 1976-1979 freshening period, when an eastward movement of the Polar Front seemed to have been responsible for the advection of freshwater from the west. The highest upper layer salinities occurred in years preceding and during times of deep convection. It seems that convection was very active before initiation of the GISA in the Greenland sea. It should be noted that the largest freshening due to surface fluxes occurred in 1966-68, 1973, 1975, 1981, 1983, and 1985, corresponding with the years of the largest ice export events.

The cumulative temperature curve showed a large interannual variability and the extreme winter cooling of 1967. Other strong winter cooling occurred in 1961, 1962, 1968, 1974, and 1975, when wintertime ice concentration was lower than usual, and very strong winds occurred, which resulting in large interannual variations in the amplitude of the wind stress. Thus freshwater could be effectively mixed in the upper water column.

Chapter 3

Model description

The thermodynamic-dynamic sea ice model used in the present study is that developed by Tremblay and Mysak (1997), who introduced a granular material rheology for the dynamic component. The thermodynamic component is a zero-layer thermodynamic model (Semtner, 1976a, see chapter 2). The sea ice model is coupled to a thermodynamic one-layer atmospheric model, and a mixed layer ocean model, which includes a prescribed horizontal circulation overlying a deep ocean at rest (see Tremblay and Mysak (1997) for further details). The continents are represented by a 6-m thick layer of conducting material. The computational grid used to represent the Arctic Ocean and surrounding seas (see Figure 3.1) is cartesian with a resolution of 111 km on a polar stereographic projection of the physical domain.

For large-scale simulation of the Arctic sea ice cover forced by monthly averaged wind stress, both the advection and acceleration terms can be neglected in the sea ice momentum balance equation. Under this approximation, the two-dimensional horizontal motion of sea ice can be described by

$$-\rho_i h f \boldsymbol{k} \times \boldsymbol{u}_i + A(\boldsymbol{\tau}_a - \boldsymbol{\tau}_w) + \nabla \cdot \boldsymbol{\sigma} - \rho_i h g \boldsymbol{\nabla} H_d = 0, \qquad (3.1)$$

where ρ_i is the sea ice density, h the mean ice thickness over a grid cell, f the Coriolis parameter, $\boldsymbol{k}$ an upward unit vector normal to the ice surface, $\boldsymbol{u}_i$ the ice velocity, A the ice concentration (percentage of a grid cell covered by ice), $\boldsymbol{\tau}_a$ the wind shear

stress on the top ice surface, $\boldsymbol{\tau}_w$ the ocean drag on the bottom of the sea ice flow, σ_{ij} ($\boldsymbol{\sigma}$) the vertically integrated internal ice stress (normal and/or shear) acting on a plane which is perpendicular to the i-axis and in the j-direction, g the gravitational acceleration and H_d the sea-surface dynamic height. Following Gray and Morland (1994), the wind stress and water drag are multiplied by the ice concentration to account for the fact that water may be present in a grid cell. The air ($\boldsymbol{\tau}_a$) and water ($\boldsymbol{\tau}_w$) stresses are obtained from a simple quadratic law with constant turning angle (McPhee, 1975), *viz.*,

$$\boldsymbol{\tau}_a = \underbrace{\rho_a C_{da} |\boldsymbol{u}_a^g|}_{C'_{da}} (\boldsymbol{u}_a^g \cos\theta_a + \boldsymbol{k} \times \boldsymbol{u}_a^g \sin\theta_a), \tag{3.2}$$

$$\boldsymbol{\tau}_w = \underbrace{\rho_w C_{dw} |\boldsymbol{u}_i - \boldsymbol{u}_w^g|}_{C'_{dw}} \left[(\boldsymbol{u}_i - \boldsymbol{u}_w^g) \cos\theta_w + \boldsymbol{k} \times (\boldsymbol{u}_i - \boldsymbol{u}_w^g) \sin\theta_w \right]. \tag{3.3}$$

where ρ_a and ρ_w are the air and water densities, C_{da} and C_{dw} the air and water drag coefficients, $\boldsymbol{u}_a^g$ and $\boldsymbol{u}_w^g$ the geostrophic wind and ocean current and θ_a and θ_w the wind and water turning angles. In the above equation for the wind shear stress, the ice speed is considered small compared to the wind speed and is therefore neglected. The values of the various constants are given in Appendix A.

Considering the sea ice to behave as a granular material in slow continuous deformation, the internal ice stress $\boldsymbol{\sigma}$ can be written as follows (Tremblay and Mysak, 1997; Flato and Hibler, 1992):

$$\sigma_{ij} = -p\delta_{ij} - \eta\dot{\epsilon}_{kk}\delta_{ij} + 2\eta\dot{\epsilon}_{i,j},$$

where

$$\eta = \min\left(\frac{p \sin\phi}{\sqrt{(\dot{\epsilon}_{11} - \dot{\epsilon}_{22})^2 + 4\dot{\epsilon}_{12}^2}}, \eta_{max} \right). \tag{3.4}$$

For small deformation ($\dot{\epsilon}_1, \dot{\epsilon}_2$), the coefficient of friction is constant ($\eta = \eta_{max}$) and sea ice behaves as a very viscous fluid. In the above equation, the pressure p cannot exceed the maximum value P_{max}, which is a function of the local ice thickness and

concentration. This can be parameterized as follows (Hibler, 1979):

$$P_{max} = P^* h \exp[-C(1-A)],$$

where P^* is the ice strength per meter ice thickness and C is the ice concentration parameter, and A is the ice concentration.

The ice strength in this model is a function of both the mean ice thickness h and ice concentration A. For this reason, a conservation law for each quantity is necessary:

$$\frac{\partial h}{\partial t} + \nabla \cdot (h \boldsymbol{u}_i) = S_h + K_h \nabla^2 h, \tag{3.5}$$

$$\frac{\partial A}{\partial t} + \nabla \cdot (A \boldsymbol{u}_i) = S_A + K_A \nabla^2 A, \tag{3.6}$$

where K_h and K_A are the diffusion coefficients for ice thickness and concentration, and S_h and S_A are the thermodynamic source terms which are given by:

$$S_h = \frac{1}{\rho_i L_f} \begin{cases} A\,(Q_{ia} - Q_{oi}) + (1-A)\,Q_{oa}, & T_o = T_{of},\ Q_{oa} > 0 \\ A\,(Q_{ia} - Q_{oi}), & \text{otherwise} \end{cases} \tag{3.7}$$

$$S_A = \frac{1}{\rho_i L_f} \begin{cases} (1-A)\,Q_{oa}/h_0, & T_o = T_{of},\ Q_{oa} > 0 \\ A\,\rho_i L_f S_h / 2h, & S_h < 0 \end{cases} \tag{3.8}$$

where L_f is the latent heat of fusion, Q_{ia} and Q_{oa} the net ice and oceanic heat fluxes to the atmosphere due to longwave ($Q_{lw-up}, Q_{lw-down}$), sensible (Q_{sens}), latent heating (Q_{lat}) and shortwave radiation (Q_{sw}) (see figure 3.2), Q_{oi} the sensible heat flux from the water to the ice, h_0 a fixed demarcation thickness between thin and thick ice (Hibler, 1979), and T_o and T_{of} the temperature and freezing point temperature of the ocean. In equation (3.6), ice concentration is restricted to lie between zero and one by using a mechanical sink term; that is, when the ice concentration A reaches its maximum value, A is capped to 100% and any further convergence motion will cause the ice thickness to increase for the internal ice pressure p exceeding the critical value P_{max}.

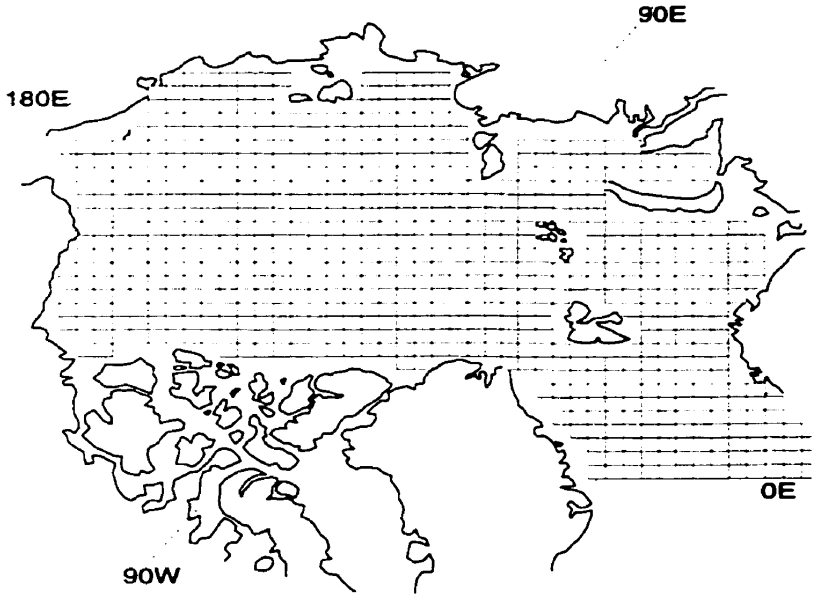

Figure 3.1: Model grid as used in Tremblay and Mysak (1997).

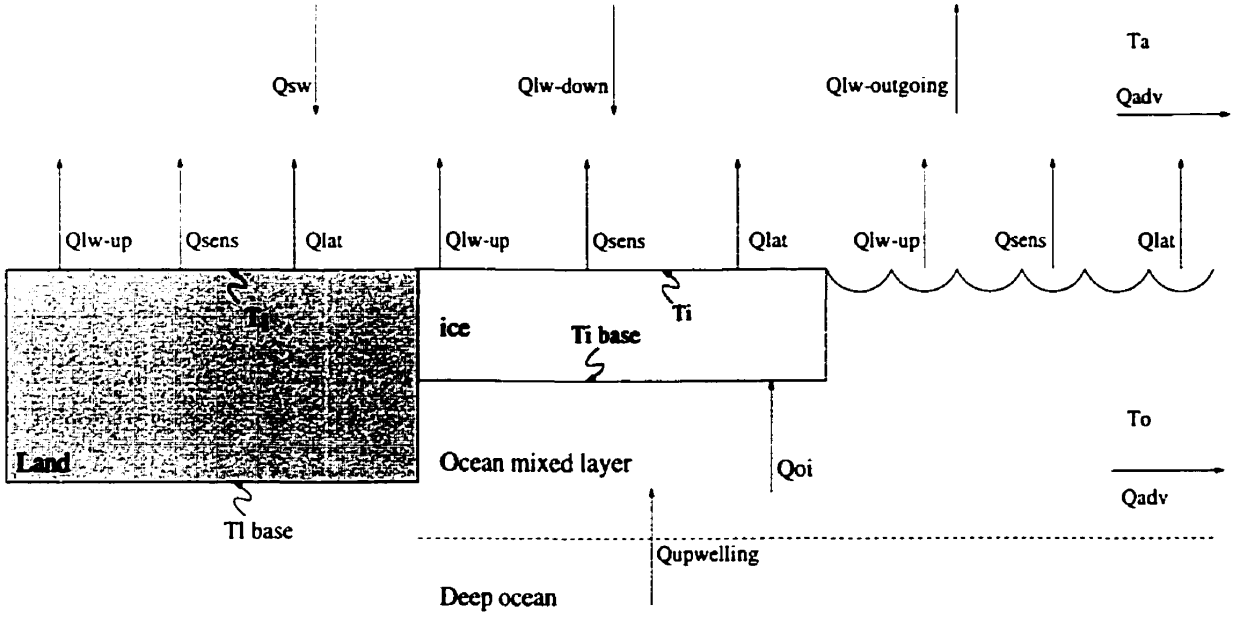

Figure 3.2: Heat fluxes over a grid cell, and the land-ice-ocean configuration as used in Tremblay and Mysak (1997).

Chapter 4

Data and methodology

4.1 Meteorological and oceanic forcing data

In the present study two different data sets were used for the atmospheric forcing: one from the National Meteorological Center (NMC), and the second from the National Center for Environmental Prediction (NCEP), both based in Washington D.C. Initially only the NMC data set was available for a long enough duration (the 36-year period 1954-1989) in order to perform a long-term climate variability study; however after this study began, the NCEP Reanalysis data set became available for the 41-year period 1958-1998.

Using the NMC data set, the daily surface temperatures at 1013 mb were first computed on the model grid from the NMC temperatures at 850 mb and the mean temperatures over the 1013 mb-850 mb layer on the NMC Octagonal grid, assuming a linear temperature profile in this layer. Then climatological monthly mean surface temperatures were obtained from the above daily temperatures. The geostrophic daily winds on the model grid were derived from the 1954-89 NMC sea level pressure analysis given on the NMC Octagonal grid. Then the daily wind stresses were computed from these geostrophic daily winds, from which were obtained the monthly mean wind stresses. Next experiments and the analysis of the results were conducted using these atmospheric forcing data for the 36-year period 1954-1989.

When the NCEP Reanalysis data set became available for the 41-year period 1958-1998, the same calculations were repeated for the longer period. The existence of the more up-to-date forcing fields was helpful since data became available for the sea ice export through Fram Strait and the mean ice thickness and mean ice velocity in the Fram Strait region for the six-year period August-1990-August-1996 (Vinje *et al.*, 1998). Therefore, it became possible to make relevant comparisons between model calculations and observations. (The previous data set was only available until 1989). For the second set of interannual calculations, the NMC data set was used for a simulation of the 4-year period 1954-1957 in order to set up the model with more realistic initial conditions for the long 41-year run beginning in 1958 using the NCEP Reanalysis data set.

As was done with the NMC data set, the monthly mean wind stresses on the model grid were obtained from the 1958-98 NCEP Reanalysis daily-averaged sea level pressure on a latitude-longitude grid. The climatological monthly mean air temperatures were obtained on the model grid from the NCEP Reanalysis daily air temperature at a height of two meters on a Gaussian grid.

For the overlapping period of the two data sets (1958-89) the sea level pressure fields are quite similar. Not surprisingly, the computed climatological monthly mean winds and the monthly mean wind stresses are also quite similar. But non-negligible differences were noticed between the two air temperature data sets. The NCEP Reanalysis air temperatures are in general colder than the surface air temperatures extrapolated from the NMC data set (see Figure 4.1; the differences above the continents are not relevant since there is an altitude difference). The air temperature difference is the largest over the Canadian Basin (around 5-6 degrees); the difference is around 2-3 degrees in the Chukchi and Kara Sea regions. The difference is much smaller in the Barents Sea region, and the NCEP Reanalysis air temperatures are a little warmer in Norwegian Sea region. Thus depending on which air temperature forcing fields are used, the ice thickness over the domain can change drastically, and hence affect the ice export through Fram Strait (see Figure 4.2). But the ice edge

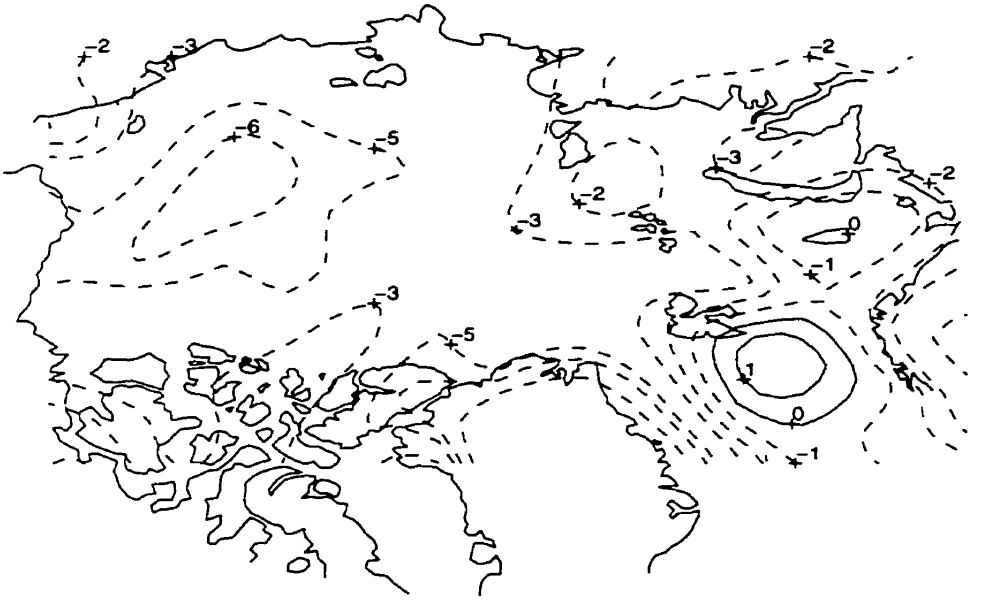

Figure 4.1: Air temperature differences: climatological NCEP Reanalysis air temperature field minus climatological NMC air temperature field.

position is not noticeably affected by the use of either temperature data set, only in the Kara Sea is the ice edge farther south with the colder air temperature field. The temperature difference between the two data sets could be due to existing inversions not considered in the calculation of the NMC temperature fields.

The choice of which air temperature data to use for forcing was made by considering the ice thickness distribution, the mean ice thickness over the domain and in the Fram Strait region obtained from our model experiments, keeping the physical parameters (ice albedo, ice strength per meter ice thickness, water and air drag coefficients, *etc.*) in realistic ranges. Over the Arctic basin the mean ice thickness is estimated to be around 3 meters (Aagaard and Carmack, 1989). During the 1990-96 period (Vinje *et al.*, 1998), the mean ice thickness in Fram Strait region was observed to be 2.9 metres, and the mean velocity 16 cm/s. Since the results of the simulation forced with the climatological monthly mean air temperatures from the NCEP Reanalysis data set are closer to the above observed values, this data set was chosen for the experiments.

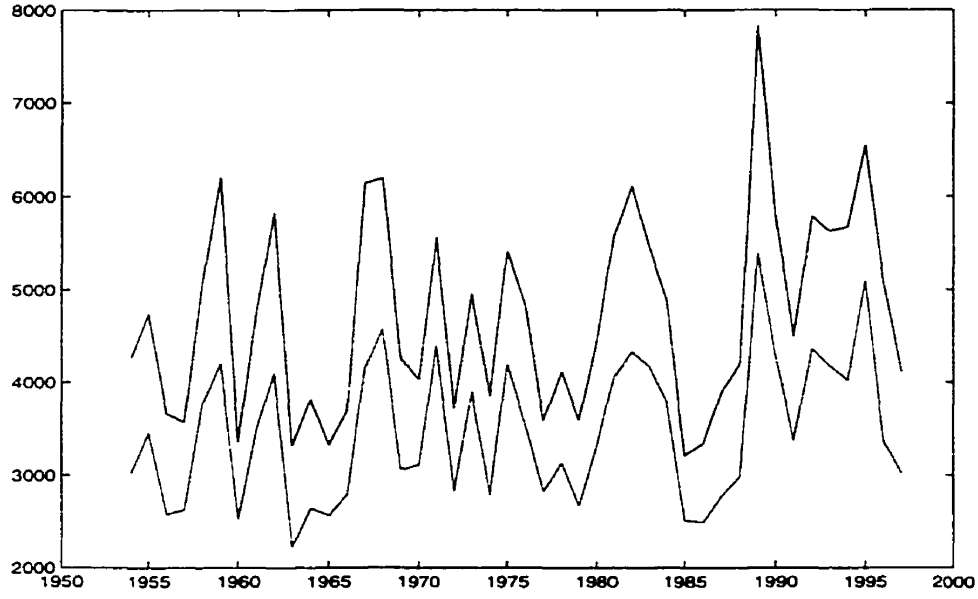

Figure 4.2: Sea ice exports through Fram Strait in km^3/yr obtained with the NMC air temperature data set (lower curve), and NCEP Reanalysis data set (upper curve).

For the ocean, the temperatures at the open boundaries are specified from monthly climatologies extracted from the Levitus Data (Levitus, 1994). The ocean currents are spatially varying but steady; they were obtained using a single-layer reduced gravity model appropriate for large scale flow (Tremblay and Mysak, 1997). The normal velocity in Berring Strait was chosen to obtain a constant inflow of 1 Sv into the Arctic Ocean. Levitus sea surface elevation data were used to specified the velocity field in the North Atlantic, the latter was scaled in such a way as to obtain no accumulation of water in the Arctic domain (Tremblay and Mysak, 1997).

4.2 Basic experiments

In order to test the different components of the model and to better understand the structure and links within it, basic experiments using a very simple domain (a rectangular basin) were performed. In this east-west oriented basin, the initial ice thickness and concentration distributions were prescribed.

The first experiments were done to test the thermodynamic part of the model. Verification that the model was able to reach a stable seasonal cycle was done by applying a seasonally varying forcing for the temperature field.

Next, the dynamic part (especially the rheology) was tested using different wind stress fields: from a wind stress due to constant westerly winds to more complex ones, such as a wind stress field calculated from a quadratic drag law. Experiments were also conducted with and without the Coriolis term, and with the different types of rheology possible in this model (free-drift conditions, cavitating rheology, granular rheology).

Since model results were able to reproduce simple analytic solutions (*e.g.*, for free-drift), and were consistent for more complex rheologies, the next step was to perform in the physical domain (see figure 4.4 below) the following experiments before doing the spin-up and the initialization of the model, and then the full model run for the 41-year period.

The first experiments in the physical domain were done using only the thermodynamic part of the model forced with the climatological monthly mean temperature.

The dynamic part of the model with and without ocean currents was tested in a second set of experiments using climatological monthly mean wind stresses and yearly mean ocean currents. Then the full model was run with the climatological monthly mean forcings to test if the model was able to reach a realistic stable seasonal cycle which could be used for the initialization of the model.

The physical parameters (see appendix A) are in realistic ranges and are comparable to the values used in other ice modelling studies (*e.g.*, Tremblay and Mysak, 1997). Instead of using parameters which yielded the observed ice export through Fram Strait like in other studies which uses a more sophisticated ocean model (Häkkinen, 1993), they were chosen to obtain consistency with the observed mean ice thickness over the domain and in the Fram Strait region, and with the observed mean ice velocity in the Fram Strait region (Vinje *et al.*, 1998). However, because the simple ocean model used in this study does not include the West Spitsbergen Current, the sea ice

export through Fram Strait is too large. This relatively warm northward current is responsible for the melting part of the outflowing sea ice in the Fram Strait region.

4.3 Spin-up and initialization of the model

Before carrying out the 41-year simulation, the model was forced with climatological data in order to reach a stable periodic seasonal cycle. Then, in order to start the 41-year run with even more realistic initial conditions, a 4-year run was conducted with the NMC data set from 1954 to 1957, starting with the above seasonal cycle simulation.

To reach the steady seasonal cycle, a 20-year run using a one-day time step was performed employing the climatological monthly mean data. The climatological monthly means are considered to represent the climatological mid-month values. The values for a particular day are obtained by a weighted average of the two closest climatological mid-month values. The climatological monthly mean data for the wind stress and the wind were obtained by taking the average over the 44-year period of the daily data from the two data sets. Because of the differences in the air temperature fields between the two data sets, only the NCEP Reanalysis data set is used to compute the climatological monthly mean temperature over the 40-year period 1958-1997.

The steady state was reached after 10 years of integration, and it was compared with the observed climatology. First, the mean sea ice thickness over the domain was computed from the spin-up results (see Figure 4.3). The value of 2.9 meters obtained agrees well with the estimated 3-m mean ice thickness (Bourke and Garrett, 1987). The mean sea ice thickness and mean sea ice velocity in the Fram Strait region were computed from the spin-up results and are respectively 2.85 metres and 15.9 cm/s; these compare very well with the observations reported by Vinje *et al.* (1998), of 2.87 metres and 16.2 cm/s, respectively.

The seasonal means of the ice thickness distribution and the ice edge position obtained from the spin-up results (see Figures 4.5a , 4.6a , 4.7a, and 4.8a) are compared

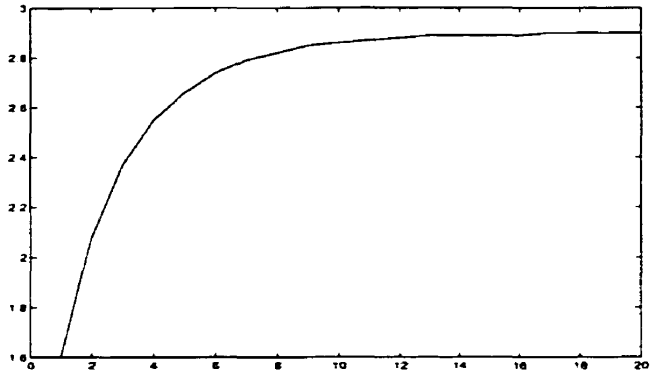

Figure 4.3: Mean ice thickness (in metres) over the domain during the 20-year spin-up.

to the sonar measurements reported by Bourke and Garrett (1987) (see figures 4.5b, 4.6b, 4.7b, and 4.8b). For the winter (January, February, and March) the modelled ice thickness contour patterns reproduce rather well the observed patterns (Bourke and Garrett, 1987). For the spring (April, May, and June), the ice contours are not in such good agreement (Figure 4.6), but the 5-m contours north of the Canadian Archipelago and north of the Greenland are still present and the 4-m contour north of Alaska is present even though located too far north. In the surrounding seas (*i.e.* Chukchi Sea, Laptev Sea, Barents Sea, and Norwegian Sea), for the two precedent seasons, and for summer (July, August, and September), and autumn (October, November, and December) the ice thickness distribution and the ice edge position are remarkably close to the observations (the ice edge position is defined as the 50% ice concentration contour). In the Beaufort Sea, the spin-up results for summer and autumn are in good agreement with the data. For winter and spring, this seems not to be the case, but the data are very sparse in time and space for this region. The ice-free region in the Laptev Sea corresponds well with the observations; this seasonal polynya is an important ice production area in the Arctic Ocean (Kassens *et al.*, 1997), right at the tail of the Transpolar Drift Stream. However, the modelled 3-m contour is too far south in the East Siberian Sea for the four seasons, and this sea is still ice-covered during summer (see Figure 4.7). The overly large sea ice extent could be due to the anomalously cold temperatures in the NCEP Reanalysis data set (T.

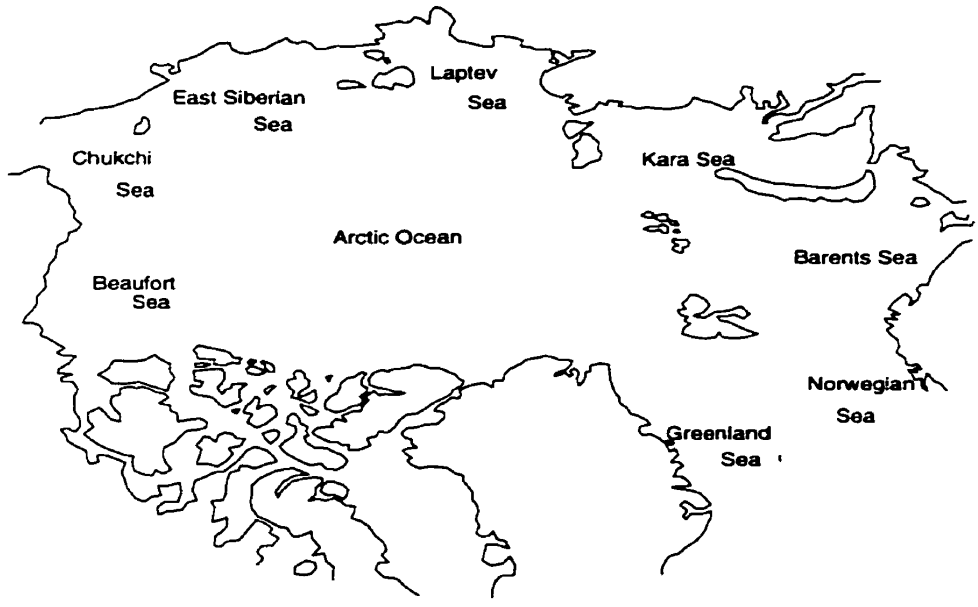

Figure 4.4: Arctic Ocean and surrounding seas. The physical domain is from Bering Strait to south of Greenland Sea (from 70°N on the east coast of Greenland to 65°N on the west coast of Norway).

Arbetter, personal communication, 1998). The same bias was observed with thinner ice (2-m contour) in the results of the simulations forced with the NMC climatological monthly mean temperatures (not shown here). For the four seasons, the one-meter contour in Kara Sea is also too far south for both simulations, but in this case it is not so far from the observed contour. It could be possible that in the two data sets, the temperatures may be too cold in these last two regions. Later the results obtained from the 41-year run (see page 38) show the importance in this problem of small scale features in time and space that are not resolved by the model and the monthly mean forcing data.

Another noticeable difference between the model and the observations for the four seasons is that the East Greenland ice edge which is too far east. This is due to the prescribed ocean currents which under-represent the recirculation of water in the Greenland Sea and do not represent the warm northward Spitsbergen Current, which would melt some of the southward flowing sea ice. For summer (see Figure

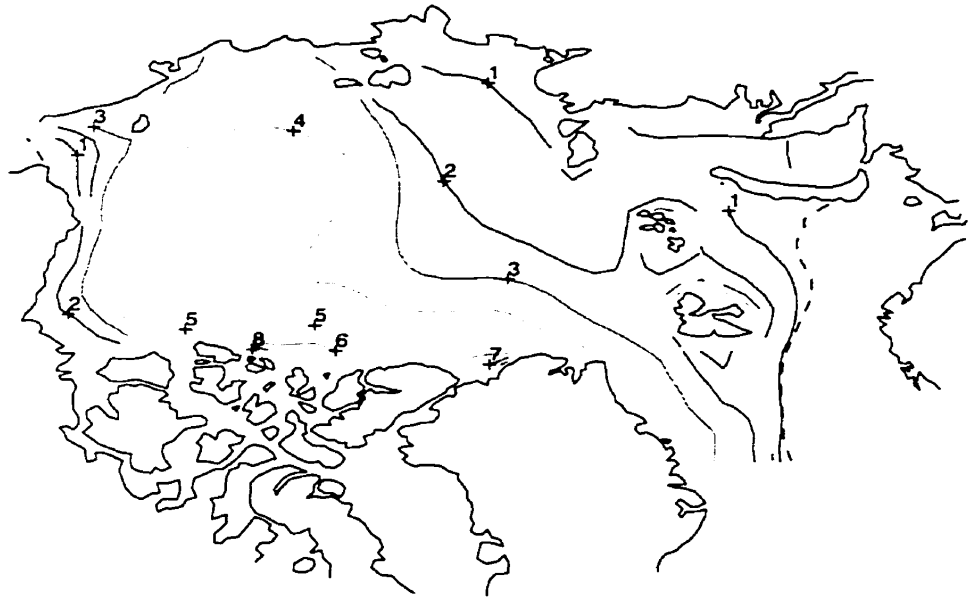

Figure 4.5: (a) Simulated winter (JFM) ice thickness distribution in meters dashed lines show the ice edge (50% ice concentration).

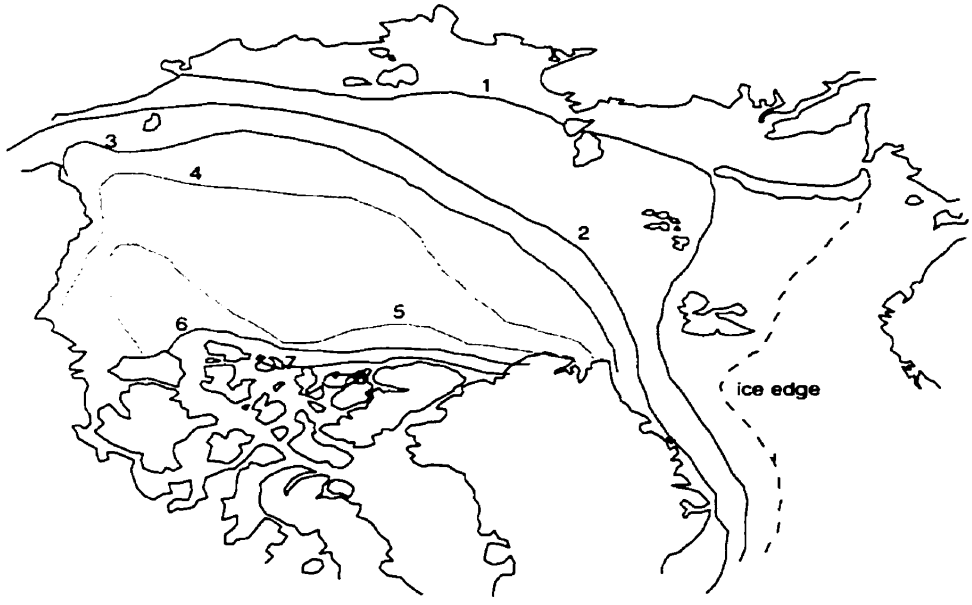

Figure 4.5: (b) Observed winter (JFM) ice thickness from Bourke and Garrett (1987).

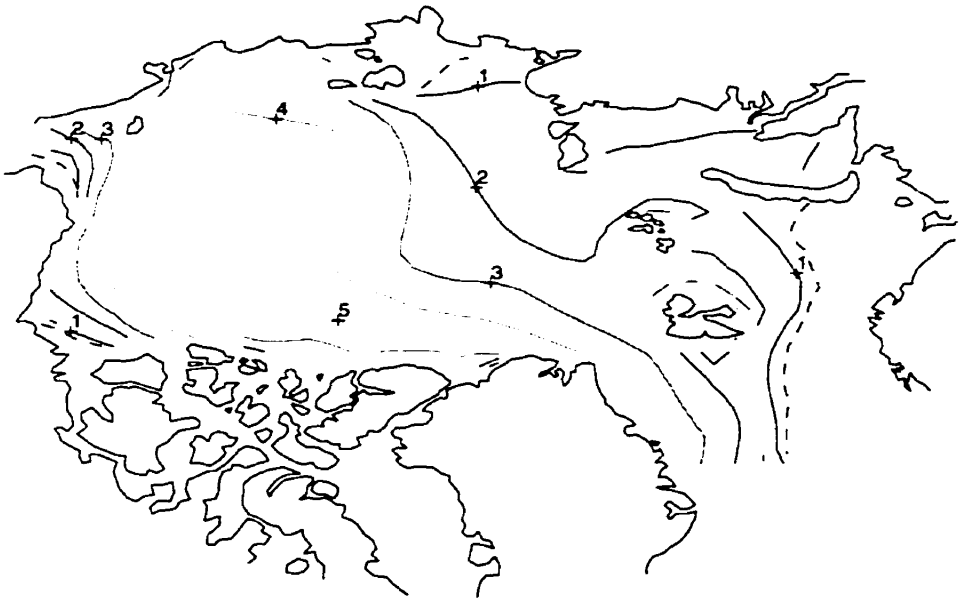

Figure 4.6: (a) Simulated spring (AMJ) ice thickness distribution in meters; dashed lines show the ice edge (50% ice concentration).

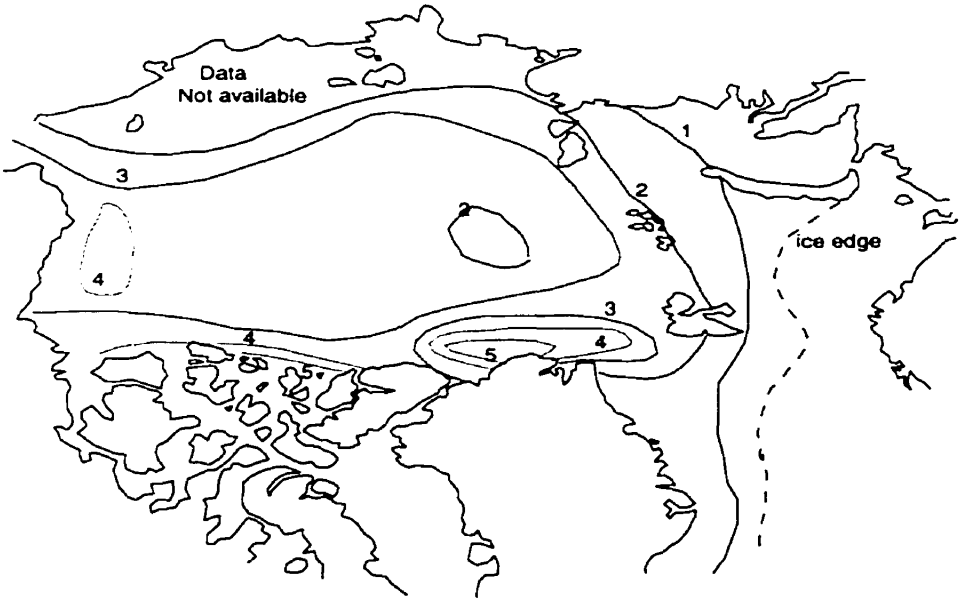

Figure 4.6: (b) Observed spring (AMJ) ice thickness from Bourke and Garrett (1987).

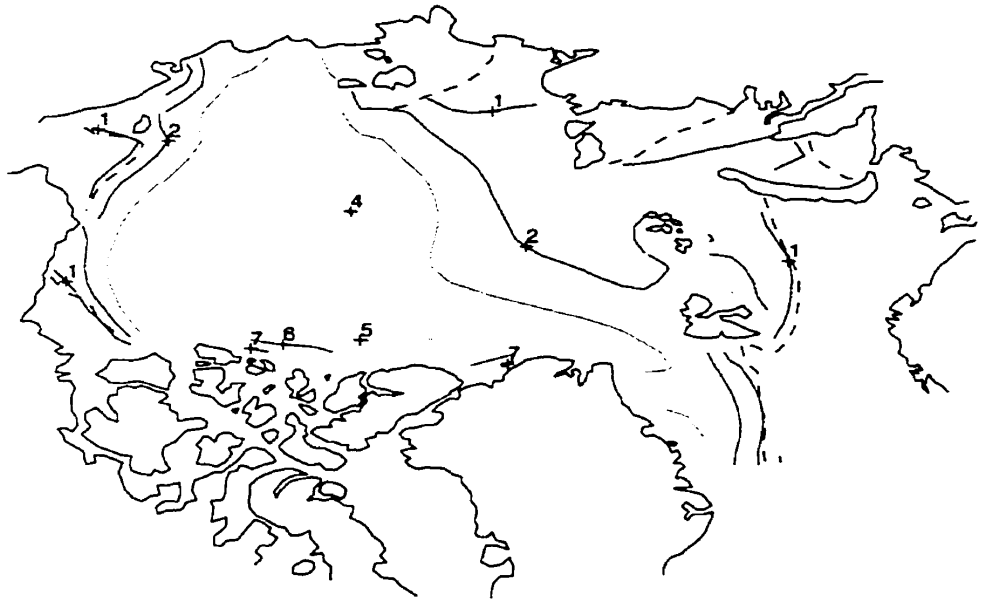

Figure 4.7: (a) Simulated summer (JAS) ice thickness distribution in meters, dashed lines show the ice edge (50% ice concentration).

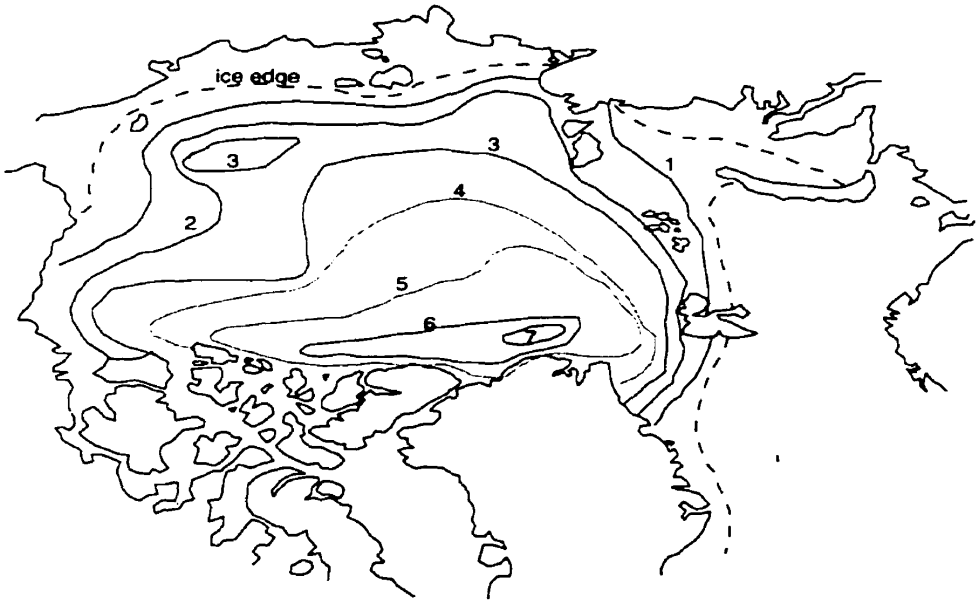

Figure 4.7: (b) Observed summer (JAS) ice thickness from Bourke and Garrett (1987).

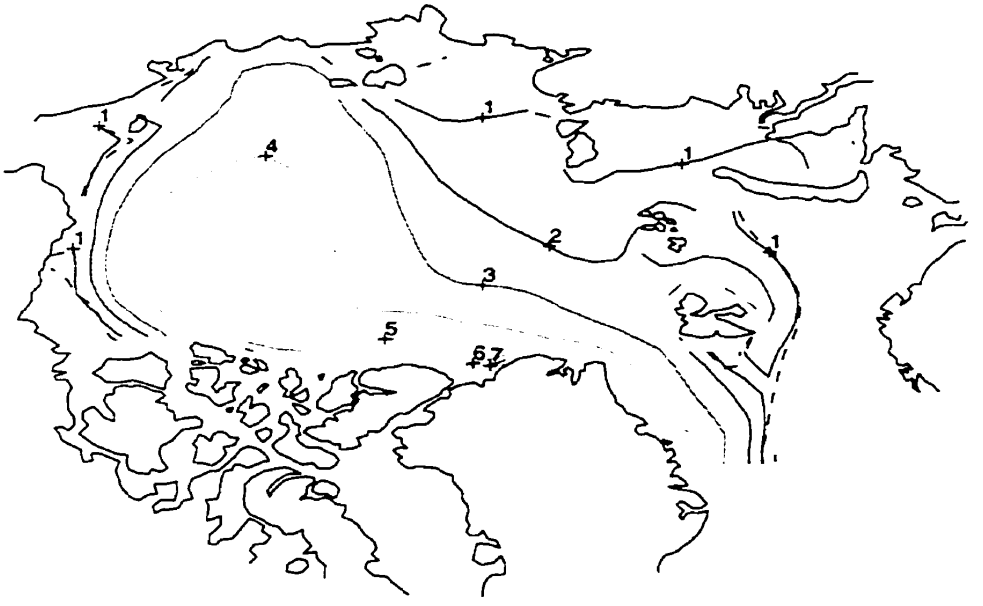

Figure 4.8: (a) Simulated autumn (OND) ice thickness distribution in meters; dashed lines show the ice edge (50% ice concentration).

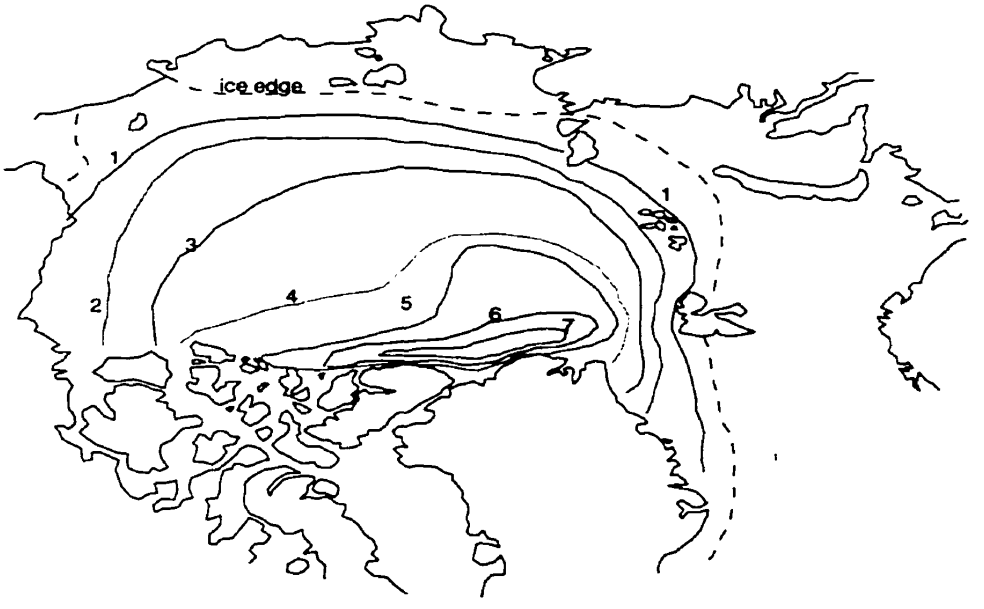

Figure 4.8: (b) Observed autumn ice (OND) thickness from Bourke and Garrett (1987).

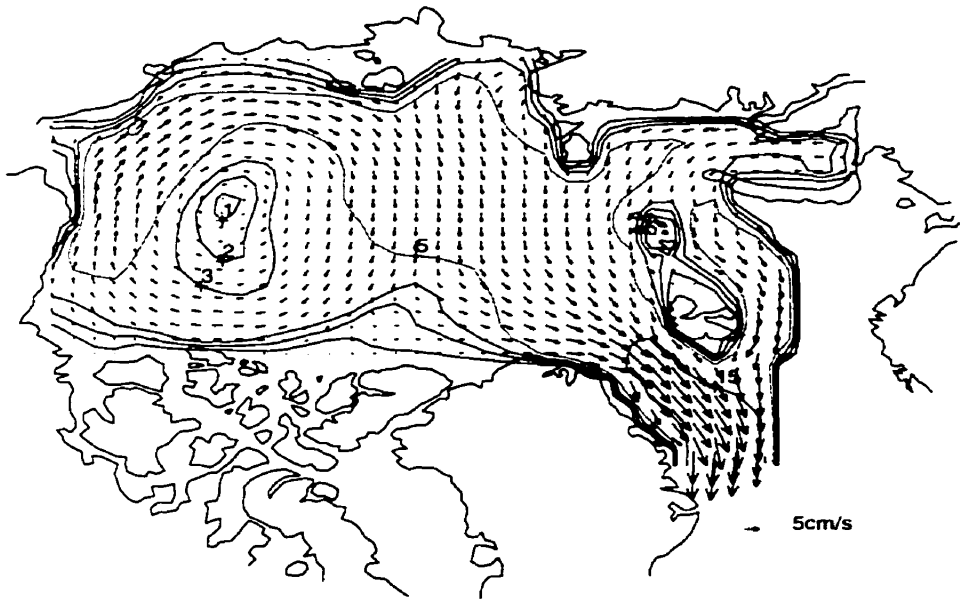

Figure 4.9: Simulated ice velocity field from the spin-up. Contours are in cm/s.

4.7). the simulated ice thickness peak is north of the Canadian Archipelago instead of north of Greenland (see Figure 4.7). The effect of the climatological wind pattern reversals in summer (McLaren *et al.*, 1987) is under-represented by the results from the climatological run. But for the same period the 7-m thick ice pattern north of Canadian Archipelago and north of Greenland is well represented.

The mean ice velocity field obtained from the spin-up of the model (Figure 4.9) is consistent with the estimation of the mean field of sea ice motion obtained by Colony and Thorndike from Arctic automatic buoy experiments (Figure 4.10). The cyclonic Beaufort Gyre is well simulated but the Beaufort Gyre is centered slightly more to the west than observed. The Transpolar Drift Stream is also well simulated and is properly positioned. There are differences in the strength of the ice velocity. The model results show slightly larger ice velocities than those in the buoy experiments in the Transpolar Drift Stream. But the observed velocities from the buoy experiments are smaller near Fram Strait than the observations reported by Vinje *et al.* (1998), *i.e.* around 16 cm/s. The simulated ice velocities in the Fram Strait region correspond

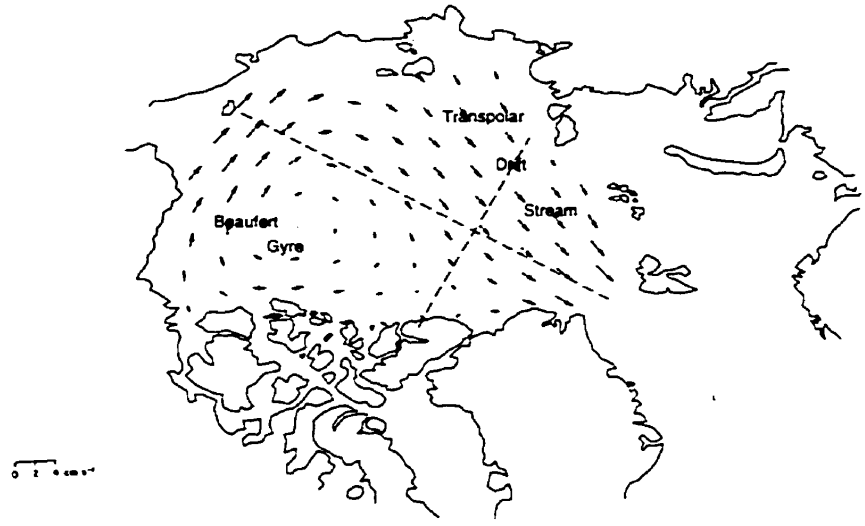

Figure 4.10: Observed annual mean velocity field from Colony and Thorndike (1984).

well with the latter.

4.4 The 41-year run

Since the goal of our study is to understand the importance of the wind fluctuations in producing interannual variability of the sea ice cover, only the monthly mean wind stress fields vary from year to year in the simulation. The air temperature and the wind used to drive the thermodynamic part of the model were set to climatological monthly means, and the ocean currents were set to the yearly mean.

The 41-year run is performed using these data with a one-day time-step. For the wind stress, the monthly mean is considered to represent the mid-month value. For the other forcings the climatological monthly means are considered to represent the climatological mid-month value. Therefore the daily values of the forcing fields are obtained by the weighted average of the two closest mid-month values. In this section we examine the climatology of the 41-year run, and compare this with the spin-up run. The year-by-year results obtained in the 41-year run will be specifically studied

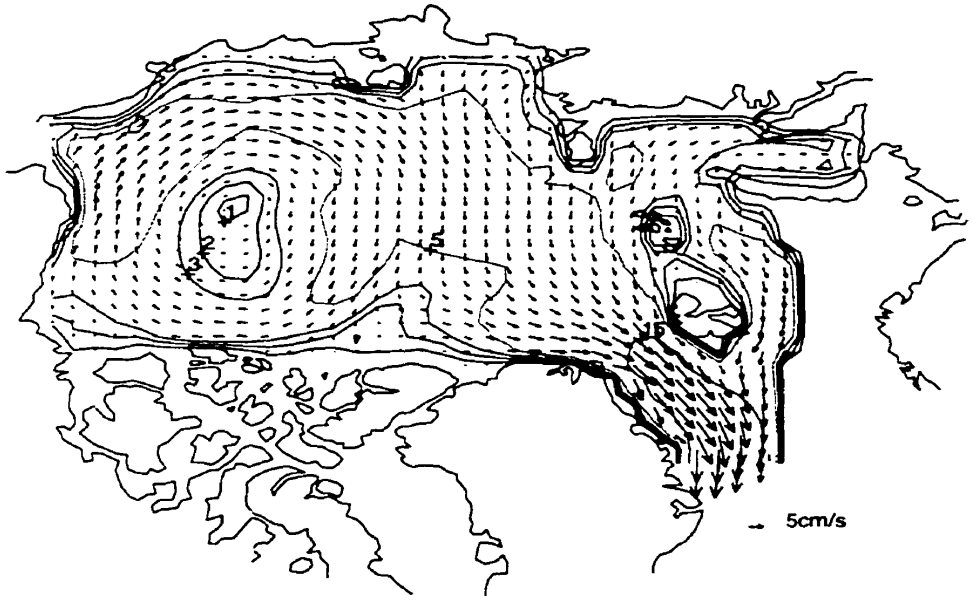

Figure 4.11: Simulated ice velocity field (41-year mean). Contours are in cm/s.

in the next chapter.

From the 41-year run results, we computed for the climatological sea ice velocity field and the seasonal ice thickness fields. The mean ice velocity field (see Figure 4.11) is very similar to the one obtained from the spin-up run (see Figure 4.9). The Beaufort Gyre is centered slightly eastward of the one obtained from the latter, but is still a little more to the west than in the observations. Also, the speed in the northern part of the Gyre in Figure 4.11 is slightly larger than in Figure 4.9, with the 5 cm/s contour being further south. It should be noted that the difference in the centre position of the Gyre between the spin-up results and the 36-year run with the NMC data set was more significant, with a Beaufort Gyre centre very close to the observed one (not shown).

For the mean seasonal ice thickness fields there are differences with the ones obtained from the spin-up results, especially for the spring and autumn. For these two seasons the mean ice thickness fields from the 41-year run are much closer to

the observations. For the spring (Figure 4.12), the pattern of the 4-m contour is well simulated, especially north of Alaska and north of Greenland. The 1-m and 2-m contours are also well simulated, as is the ice edge position. However, the latter is a little too far north in Barents Sea. The 3-m contour goes a little too far south in the East Siberian Sea; the same was true for the spin-up.

For autumn (Figure 4.13), the simulated 3-m contour is still too far south in the East Siberian Sea but not as much as in the spin-up results. This difference suggests that the utilization of mean forcing can smooth atmospheric events in this region, such as low pressure systems which occur in a too short a timescale to be realistically represented in the monthly mean forcing. Their mechanical effects of making the East Siberian Sea ice-free are under-represented in the results. The ice-free regions created in this way could allow the incoming solar radiation to warm the ocean and make the East Siberian Sea less ice covered than in the simulation results. Another possibility is that the scale of these atmospheric patterns is too small to be resolved by the model (B. Tremblay, personal communication, 1998). The 4-m contour is much more realistic, even though its peak is a little too far west, as in the spin-up results. This confirms that with less smooth forcing the results are more realistic.

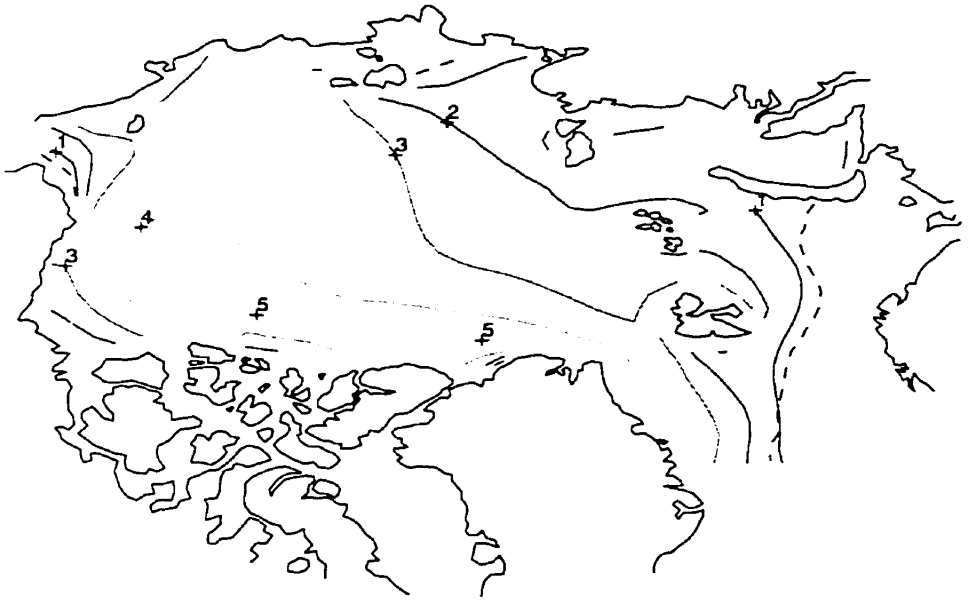

Figure 4.12: Simulated spring (AMJ) ice thickness distribution in meters (41-year mean). Dashed lines show the ice edge (50% ice concentration).

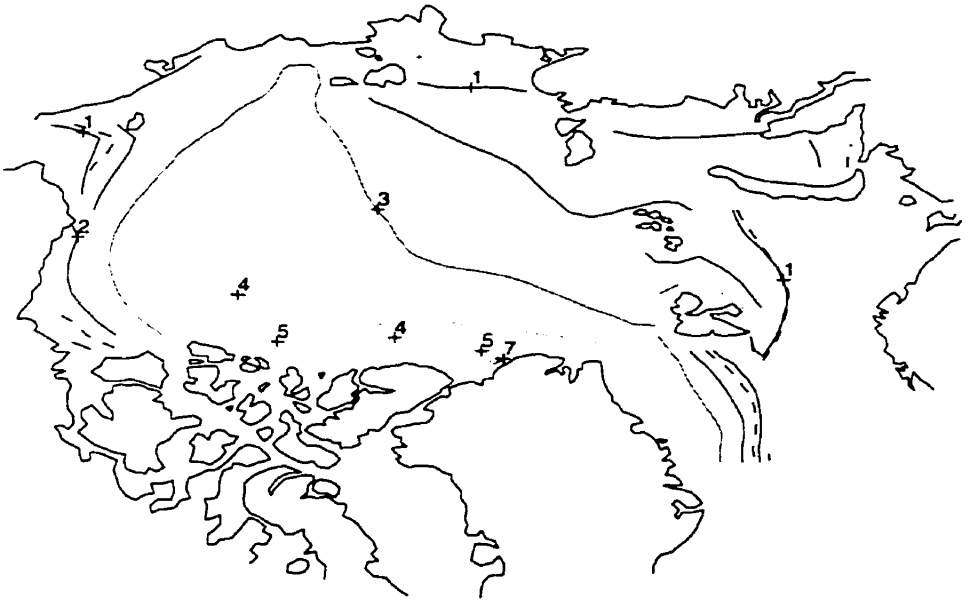

Figure 4.13: Simulated autumn (OND) ice thickness distribution in meters (41-year mean). Dashed lines show the ice edge (50% ice concentration).

Chapter 5

Sea ice cover interannual variability due to variable wind fields

The purpose of this chapter is to analyze the year-to-year variations in the results of the 41-year run. Since only the wind stress forcing varies from year to year, the sea ice interannual variability is mainly due to dynamic processes. Walsh *et al.* (1985, see chapter 2) pointed out the dominance of thermodynamic processes in producing the annual cycle in the Arctic sea ice cover, and the dominance of dynamic processes for interannual fluctuations. Other studies tend to confirm this conclusion. For example, Maslanik and Dunn (1997) showed that interannual variability in mean ice extent and ice volume is primarily due to the wind driven sea ice transport.

Sea ice transport out of the Arctic Basin is also an important quantity to consider. Most of this transport is through Fram Strait; of the total, less than 5% passes through the Canadian Archipelago straits and less than 1% passes out via the Barents Sea (Alekseev *et al.*, 1997). Mauritzen and Häkkinen (1997), using a fully prognostic coupled ocean-ice model, showed the significant role played by the sea ice export

through Fram Strait in determining the strength of the overturning cell (thermohaline circulation, THC) in the North Atlantic Ocean. Their results show that winds and ocean currents transport annually 40% of the Fram Strait sea ice export through Denmark Strait and further into the subpolar gyre. The Labrador Sea branch of the meridional overturning cell is shown to be particularly sensitive to the changes in sea ice export. The dense water export across the Greenland-Scotland Ridge is less sensitive to the sea ice variations. Nevertheless, the results of Mauritzen and Häkkinen (1997) show that the range of variability in the THC induced by sea ice variations can reach 5-6 Sv. These results further motivate our desire to examine the interannual variability of the sea ice export through Fram Strait in the next two sections (5.1 and 5.2).

5.1 Validation of the sea ice export anomalies through Fram Strait

Despite the over-estimate of the mean sea ice export through Fram Strait due to the ocean model used in this study, the mean sea ice thickness and velocity fields in the Fram Strait region are realistic (see chapter 4). Therefore, we first wish to determine whether the anomalies of the sea ice export through Fram Strait are realistic.

The first comparison was made with the results of Häkkinen (1995) obtained from a 26-year run (1960-1985) forced with daily winds, which were derived from the National Center for Atmospheric Research sea level pressure analysis and climatological air temperatures (see chapter 2). We computed the departures from the respective means for both simulations to obtain the sea ice export anomalies (see Figure 5.1.).

For the overlapping period (1960-1985), the sea ice export anomaly peaks are very well correlated (r=0.89), and the departures from the mean are comparable. However, some differences are noticeable; the low sea ice export period in the mid 1960's is lower

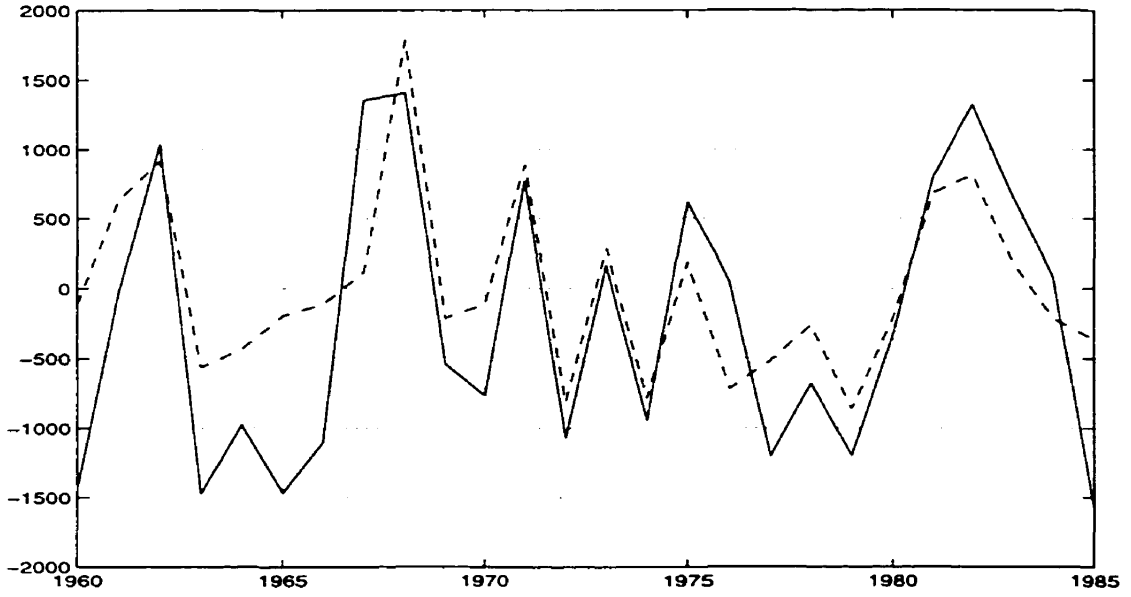

Figure 5.1: Comparison of anomalies in sea ice export through Fram Strait in $km^3/year$: results from our 41-year run (solid line) versus those from the Häkkinen (1995) 26-year run (dashed line).

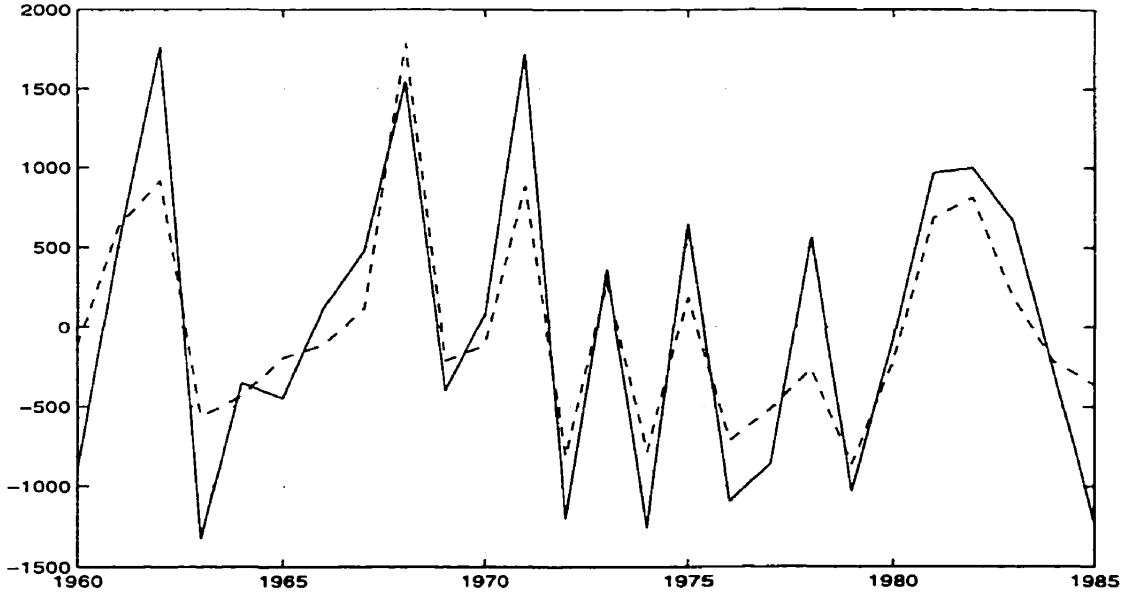

Figure 5.2: Comparison of anomalies in sea ice export through Fram Strait in $km^3/year$: results from our 36-year run (solid line) using NMC data set (for the wind stress and the air temperature) versus those from the Häkkinen (1995) 26-year run (dashed line).

in our model results, and the following large export in 1968 is slightly weaker and starts earlier, and therefore extends over a longer time period (*i.e.*, 1967-68). This large sea ice export is thought to be the origin of the GISA event (see chapter 1 and Häkkinen, 1993, discussed in chapter 2). Our modelled sea ice export anomalies are a little larger in 1975 and in 1982, and the latter export lasts longer than in the Häkkinen results.

The results from the 36-year run forced with the NMC data set (Figure 5.2) also gives larger exports in 1975 and at the beginning of the 1980's and a slightly lower export in 1968 than Hakkinen (1995). The peaks in the two time series, however, are also well correlated (r=0.77). The NMC run showed much larger amplitude events than in the Häkkinen results for some other events (*i.e.* 1962, and during the 1970's). Therefore, the updated forcing fields seem to improve the results.

The more recent forcing fields also allow a comparison with observed sea ice export through Fram Strait for the six-year period from August 1990 to August 1996 (Vinje *et al.*, 1998). The observed mean ice export during this period was 2875 km^3/yr. This value is consistent with the 2800 km^3/yr estimated by Aagaard and Carmack (1989), but not with the mean sea ice export of 4835 km^3/yr estimated by Alekseev *et al.* (1997) using the 1976-84 observations by Vinje and Finnekasa (1986). The latter value seems to have a bias and was revised downward by Smirnov and Smirnov (1998) to a mean value of 2800 km^3/yr. As explained earlier our calculated mean export is also too high; for the same 6-year period the mean modelled sea ice export was computed to be 5600 km^3/yr (see Figure 5.3). This mean sea ice export over the 41 year period was subtracted from the sea ice export obtained during this 6-year period to obtain the anomaly export for this period. Then the observed mean sea ice export over the 6-year period was subtracted from the observed sea ice export to obtain the observed anomaly export.

The above departures have the same order of magnitude (see Figure 5.4). The

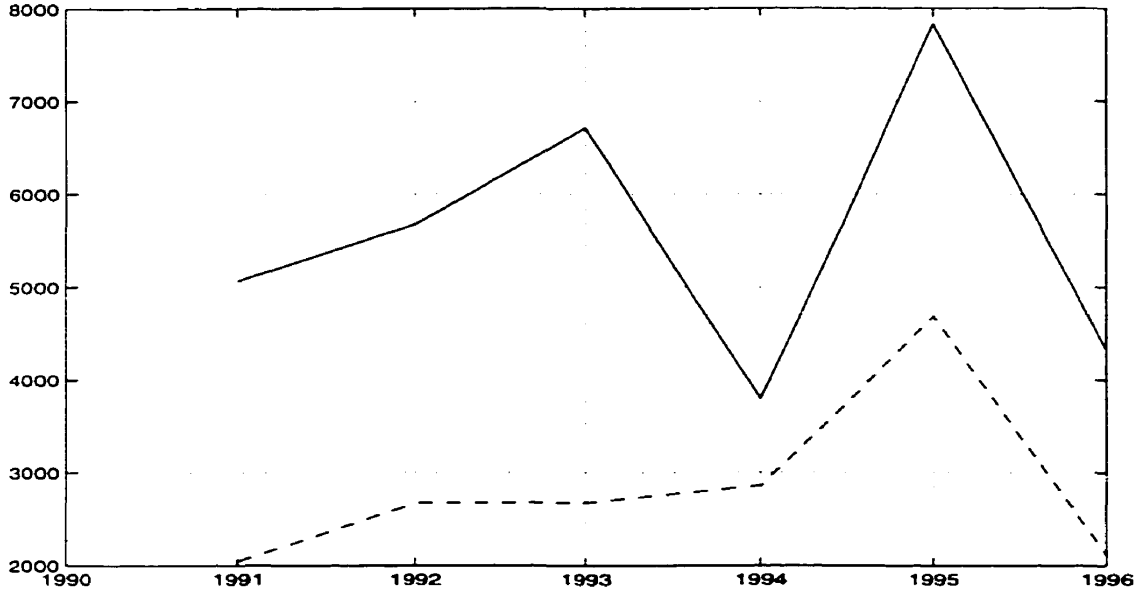

Figure 5.3: Sea ice export through Fram Strait in km^3/yr from August 1990 to August 1996: model results (solid line) versus Vinje *et al.* (1998) observations (dashed line).

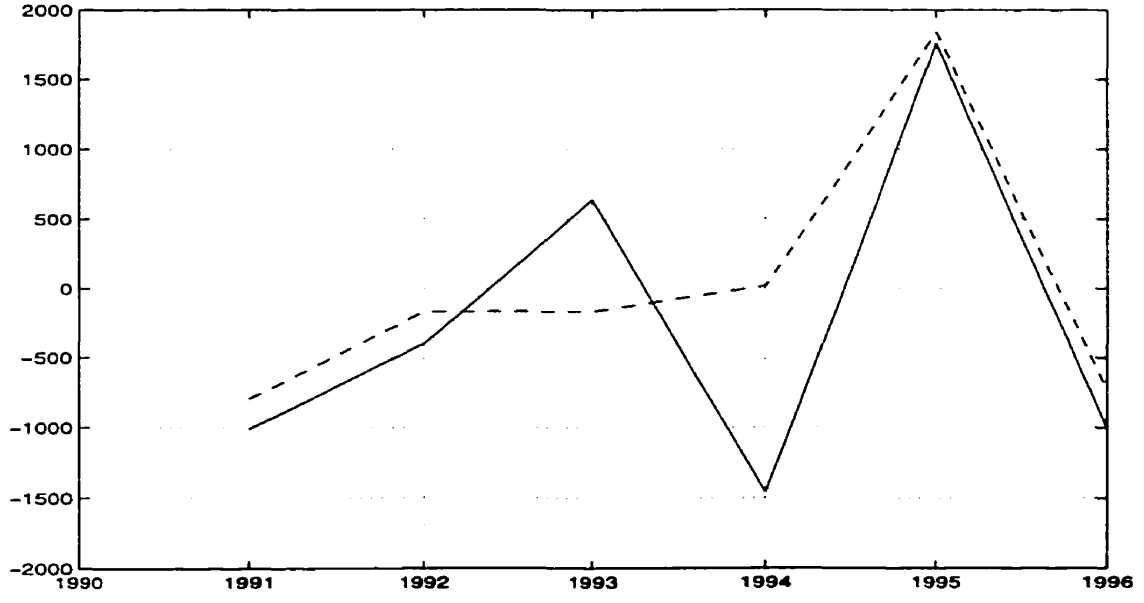

Figure 5.4: Sea ice export anomaly through Fram Strait in km^3/yr from August 1990 to August 1996: model results (solid line) versus Vinje *et al.* (1998) observations (dashed line).

slope of the increasing export during the first year of the observations is the same as in the model results. The largest export occurs during the period from August 1994 to July 1995 and is well represented in the model results. The two other model anomalies for the periods from August 1992 to July 1993 (positive) and from August 1993 to July 1994 (negative) are not seen in the observations, but their means correspond to the observed values. It should be noted that in the model results for the period from August 1992 to July 1993, the sea ice is a little thicker than observed, and for the period from August 1993 to July 1994 the sea ice velocity is a little smaller than observed.

In the simulation, the air temperature does not vary from year to year; also, the variability in the strength of the West Spitsbergen Current and the variability of heat transported by it (see chapter 2, Hibler and Walsh (1982)) can affect the sea ice thickness and the sea ice velocity in the Fram Strait region. This could counter the effect of the winds in transporting thick or fast moving sea ice southward. Despite these differences, the modelled sea ice export anomalies are quite realistic since our anomalies correspond well with those obtained using a model which includes a more complex ocean (Häkkinen, 1995), and since the results reproduce the magnitude and timing of the large observed sea ice export anomalies in 1994-1995. The largest export anomaly of 1760 km^3/yr for the 6-year period, occurring from August 1994 to July 1995, is the second largest in the 41-year simulation. The largest anomaly (3000 km^3/yr) during the 41-year period occurs in 1989 (see Figure 5.5), a year not included in the Häkkinen (1995) study.

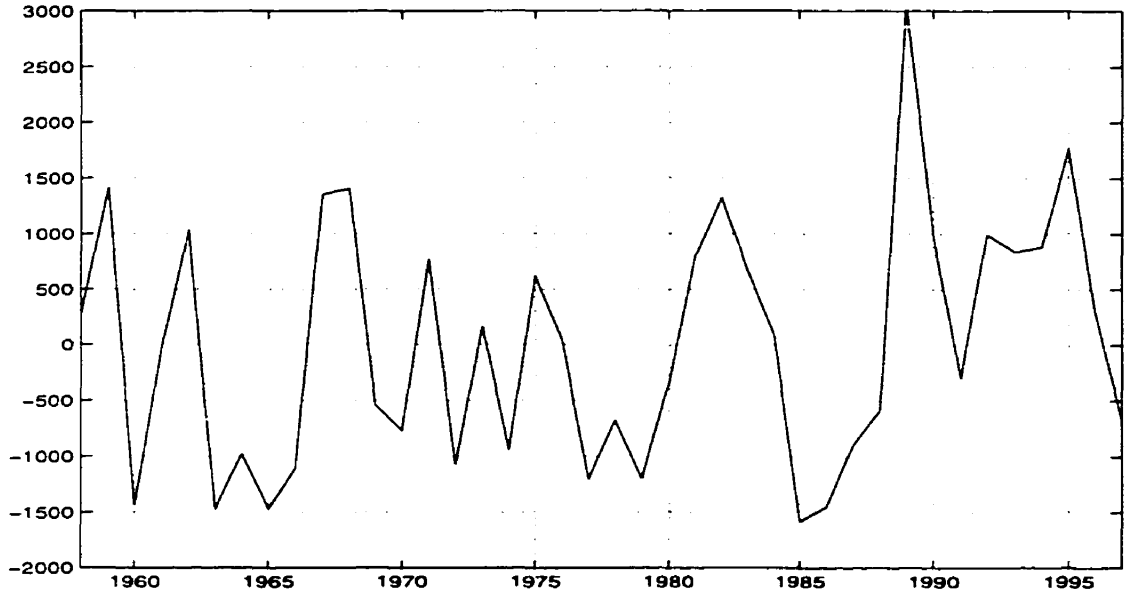

Figure 5.5: Sea ice export anomaly through Fram Strait in km^3/yr.

5.2 Interannual variability of the sea ice export through Fram Strait

The sea ice export through Fram Strait shows five large positive large anomalies (more than 1000 km^3/yr) during the 41-year period: 1969, 1967-68, 1981-83, 1989, and 1995 (see Figure 5.5). The second, third, and fourth periods are preceded by periods of large negative anomalies. These low sea ice export periods correspond to periods of increase in the sea ice volume in the Arctic Basin, and will be discussed in the next section (5.3).

Relative to the canonical mean sea ice export of 2800 km^3/yr (Aagaard and Carmack, 1989), the maxima of the first three positive anomalies are about 47% of this value, whereas the 1989 anomaly is roughly equal to the mean export value. The minima during the negative anomaly periods (1963-65 and 1985-86) are around 50% less than the mean, and 35% less than the mean (1977-78).

During the last decade, important data-based investigations were conducted to study two of these large export events (1967-68 and 1981-83) and their relation to the GISA of the 1970's (Dickson *et al.*, 1988) and the GSA of the 1980's (Belkin *et al.*, 1998). Belkin *et al.* (1998) revisited the GISA of the 1970's and documented what they call the GSAs of the 1980's and the 1980's/1990's. For the purpose of this study, we use the same terminology as Belkin *et al.* (1998) used for the events in the 1980's and 1990's, even though they were associated with large sea ice anomalies and therefore could be called Ice and Salinity Anomaly events. The authors considered the anomalies in salinity and temperature in the Labrador Sea, and investigated their origin: that is, whether they were locally created or due to salinity and temperature anomalies advected from the Greenland and Icelandic seas resulting from large ice exports through Fram Strait. From earlier publications (see Belkin *et al.*, 1998) , it was found that large sea ice extents occurred in Greenland and Iceland Seas in the late 1950's and in the late 1960's. These results agree very well with our large sea ice export anomalies in 1959 and 1967-68.

The 1967-68 sea ice export anomaly is considered to be the origin of the GISA of the 1970's. The presence of a salt deficit and negative sea surface temperature anomaly in the Iceland Sea in 1968 confirms that the positive anomaly in sea ice export through Fram Strait should start at least during the second part of 1967 (Belkin *et al.*, 1998). This is consistent with the two large exports in 1967 and 1968 (see Figure 5.5).

Dickson *et al.* (1988) estimated that the salt deficit which advected through Labrador Sea in the beginning of the 1970's was equivalent to a fresh water excess of 2000 km^3 in Labrador Sea. The results of the 41-year run show an anomaly just under 1500 km^3/yr during the two years 1967 (1353 km^3 during the second half 1967) and 1968 (1405 km^3 during the first half 1968). Thus, the total amount of excess sea ice export is 2732 km^3. Considering a mean sea ice export of 2800 km^3, this is equivalent

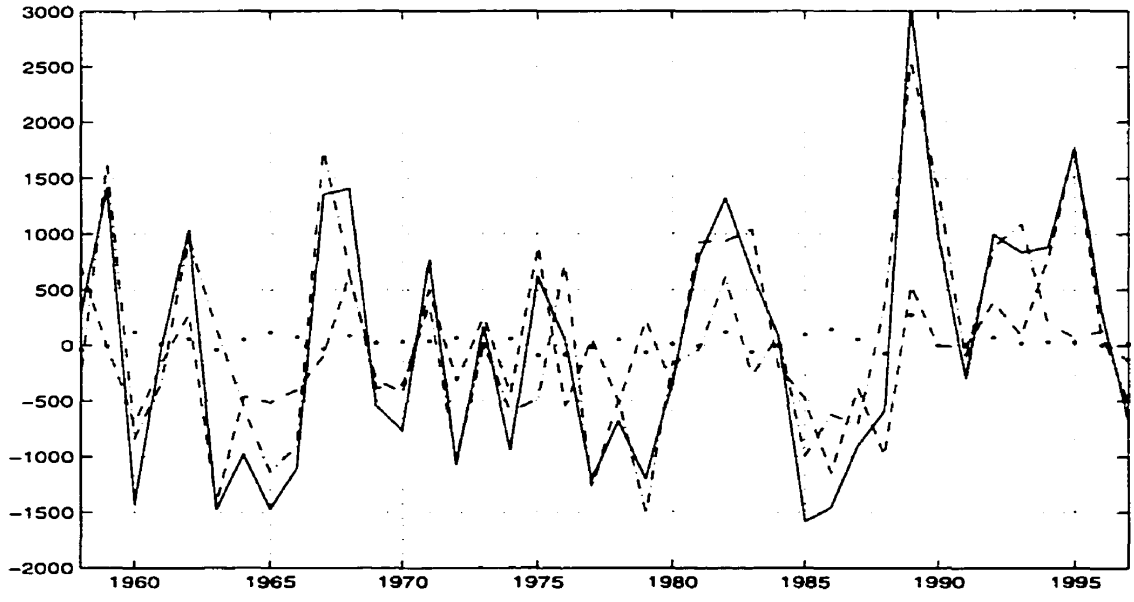

Figure 5.6: The sea ice export anomaly through Fram Strait in km^3/yr (solid line) decomposed into $h'v'$ (dotted line), $v'\overline{h}$ (dashed line), and $h'\overline{v}$ (dash-dotted line).

to an total export of 5532 km^3. It is interesting to note that 36% of this total sea ice export, yields a value of 2000 km^3, which is comparable to the fresh water excess required in the Labrador Sea. Mauritzen and Häkkinen (1997) showed that around 40% of the Fram Strait sea ice export is transported through Denmark Strait into the subpolar gyre. Therefore, the excess of sea ice export through Fram Strait during the 1967-68 period can explain the salinity negative anomaly in Labrador Sea during the 1969-70 period and therefore can be the origin of the GSA of the 1970's.

The sea ice export through Fram Strait is proportional to the product of the sea ice thickness and velocity in this region. Thus, the sea ice export anomaly for the 41-year period can be decomposed into the mean values and anomalies of (see Figure 5.6) the sea ice thickness ($\overline{h}$ and h') and sea ice velocity ($\overline{v}$ and v') in the Fram Strait region. Mathematically, the sea ice export anomaly is defined by

$$(hv)' = (\overline{h} + h')(\overline{v} + v') - \overline{hv} = \overline{h}\overline{v} + h'\overline{v} + v'\overline{h} + h'v' - \overline{hv} \tag{5.1}$$

Taking the average of (5.1) yields

$$0 = \overline{h'v'} + \overline{h}\overline{v} - \overline{hv} \tag{5.2}$$

The quantity $\overline{h'v'} = \overline{hv} - \overline{h}\overline{v}$ was computed and was found to be close to zero (less than 1% of the mean observed sea ice export). Therefore, to within 1%, $\overline{hv} = \overline{h}\overline{v}$ and (5.1) imply that the ice export anomaly $(hv)'$ is equal to the sum of three terms: $h'\overline{v}$, $v'\overline{h}$, and $h'v'$ multiplied by a constant (proportional to the width of Fram Strait).

The first interesting results from this decomposition are that the product $h'v'$ is not significant, and that h' and v' are not correlated, since the product $h'v'$ is small and is sometimes positive and sometimes negative. Therefore, there is no direct relation between the sea ice thickness anomaly and velocity anomaly in the Fram Strait region. The two other terms indicate that for the two previously considered large events (1959 and 1967-68), the anomaly in the export was mainly due to thicker than usual sea ice. This result is in agreement with those obtained by Häkkinen (1993), as reviewed in chapter 2.

This latter result also establishes that the strength of the northerly wind in the Fram Strait region is not necessarily the dominant factor in producing anomalies of sea ice export. The northerly wind stress anomaly computed for the 41-year period confirms this result (Figure 5.7). For example, during the 1967-68 large export period, the northerly wind anomaly only became larger in 1968, in the second year of this large export period, and thus played an important role in the export in 1968 only. This is confirmed by the greater importance of the $v'\overline{h}$ term (Figure 5.6) in 1968; the $h'\overline{v}$ term confirms that in 1967 the large export was due to the thickness anomaly. This shows the importance of knowing the sea ice behaviour and distribution inside

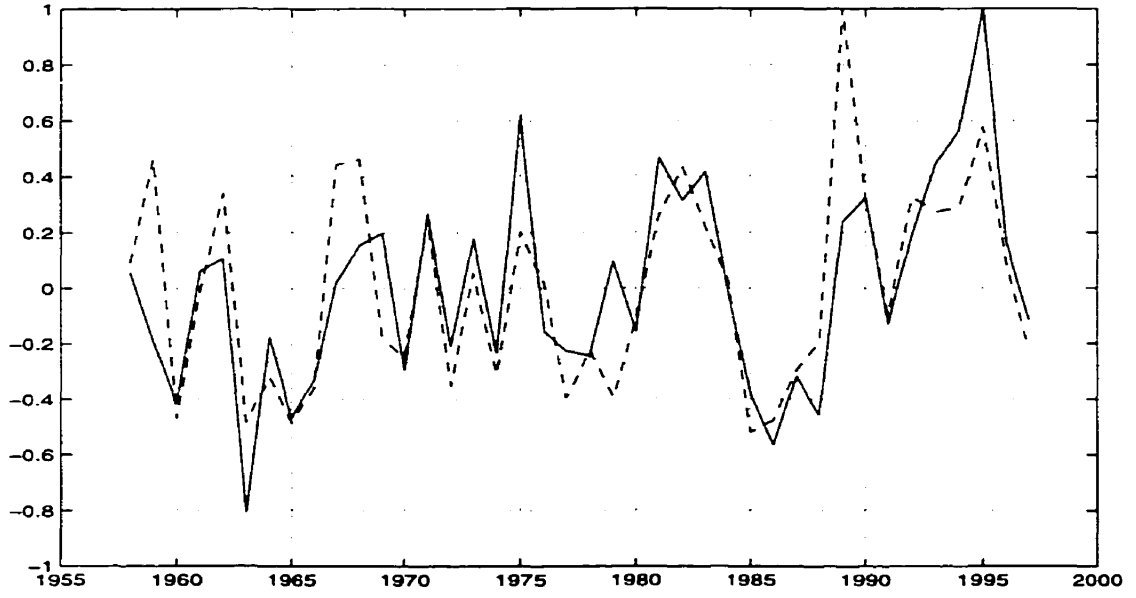

Figure 5.7: Normalized northerly wind stress anomaly in Fram Strait region (solid line) versus normalized sea ice export anomaly through Fram Strait (dashed line).

the Arctic Basin before it is to be exported through Fram Strait, a feature pointed out by Walsh and Chapman (1990).

Belkin *et al.* (1998) believe the origin of the GSA of the 1980's to be different than the origin of the GISA of the 1970's. They argue that no large sea ice extent was observed in the Greenland Sea at the end of the 1970's and the beginning of the 1980's. Therefore, the GSA of the 1980's would not be explained by an anomalously large sea ice export through Fram Strait. However, there are negative salinity and temperature anomalies in the Iceland Sea during the 1981-83 period, but weaker than those in 1968.

Anomalously low salinity and temperature in the Labrador Sea occurred in 1982, and were greater than in 1969-70. Anomalously low air temperatures in Labrador Sea were associated with northerly winds. Belkin *et al.* (1998) argue for a local origin of the GSA of the 1980's in Labrador Sea during the early 1980's. However, a local anomalous sea ice formation in the Labrador Sea would increase the salinity of the

sea water due to brine rejection.The presence of extensive sea ice would prevent heat loss to the atmosphere, and hence prevent deep convection. Thus sea water salinity would not show as large a negative anomaly, even after ice melting.

Northerly winds in the Fram Strait region were also strong during the 1981-83 period (see Figure 5.7), and the sea ice export through Fram Strait obtained from the 41-year run is about as large as in 1967-68. But the reason for the anomalous export is different for the two periods (see Figure 5.6). The anomalous export in 1967-68 was due to thick ice (the term $h'\overline{v}$), while the anomalous export in 1981-83 was due to more rapidly moving sea ice (the term $v'\overline{h}$). The northerly winds increased later in the 1967-68 period, but were already quite strong in 1981 when the sea ice export increased.

Belkin *et al.* (1998) argue that the results of Chapman and Walsh (1993) do not show any large positive anomalous sea ice extent in Greenland Sea for the 1981-83 period which are as large as those during the 1967-68 period. Eckardt *et al.* (1992) used satellite data and considered the sea ice extent anomalies for each nordic sea. They found a negative linear trend in sea ice cover in Greenland Sea for the 1966-89 period, with however, a positive sea ice extent anomaly in 1981 as large as the one in 1968, a 1982 anomaly as large as the one in 1967, and a 1983 anomaly as large as the one in 1969. Also, anomalies in salinity and temperature in the East Greenland Current in 1981-82, considered to be the end of the GISA of the 1970's, could be the beginning of the GSA of the 1980's.

The negative anomalies of salinity and temperature in the Labrador Sea are larger in amplitude in 1982 than in 1969-70, and vice versa for the Greenland and Iceland seas. This 1982 cooling could be explained by the cold atmospheric conditions in 1982 in the North West Atlantic due to anomalously cold northerly winds. These cold atmospheric conditions could prevent the ice from melting in the Greenland and Iceland seas, suggesting that the summer sea ice extent in Greenland and Iceland seas

remain large. Anomalies in sea ice extent in the Greenland Sea obtained by Eckardt *et al.* (1992) show a larger sea ice extent during the summers of the 1981-83 period than before, but it is not clear if this is large enough to explain the origin of the 1980's GSA as being sea ice advected from the Greenland Sea.

Low salinity and temperature anomalies in the Labrador Sea occurs in 1984, and the anomalous sea ice export through Fram Strait occur during the three year 1981-83 period. The total sea ice anomaly over the 1981-83 period (largest peak is in 1982) is the same as the total sea ice anomaly during the 2-year period 1967-68, but it spreads out during three years. The sea ice export shows a much larger velocity during the 1981-83 period than during the 1967-68 period (see Figure 5.6). However, since negative salinity and temperature anomalies in Labrador Sea occurred just one year after the end of the large sea ice export period, this is not long enough to explain these anomalies in salinity and temperature.

Recently, results for the sea ice export through Fram Strait for the 1947-92 period from a statistical model based on observations have become available (A. Smirnov, personal communication, 1998). The results indicate a sea ice export anomaly of 1500 km^3 in 1981 during one of the observation periods. This confirms a large export in 1981 but not in 1982. This large export is around 3500 km^3, and 40% of this quantity can be transported to the Labrador Sea (Mauritzen and Häkkinen, 1997), corresponding to an amount is equal to 1400 km^3. This is not enough to explain the negative anomaly in temperature and salinity in the Labrador Sea in 1984 (*i.e.*, 2000 km^3 would be needed, as in the GISA event). But this export could contribute to a negative anomaly in the central Labrador Sea in 1984, and contribute significantly to the GSA of the 1980's.

The resolution of the model, however, does not allow one to consider the sea ice transport through the Canadian Archipelago. Belkin *et al.* (1998) reported recent results from other studies which tend to show that the outflow of fresh water from

the Arctic Ocean to Baffin Bay, through the Canadian Archipelago and then to the Labrador Sea is not negligible. This fresh water influx in the Labrador Sea could make an important contribution to a GSA event and even initiate the anomaly. A huge quantity of thick ice is packed along the northern Canadian Archipelago and Greenland coasts in the Arctic Basin (see sea ice thickness distribution maps in chapter 4). If a non-negligible part of this thick ice could circulate through the Canadian Archipelago straits, it would certainly have an important effect on the fresh water budget in the Labrador Sea. This feature is not represented in the present model since the Canadian Archipelago is closed.

The sea ice export anomaly in 1989 is the largest of the 1958-98 period. Mysak and Power (1992) report large sea ice extents and low salinities in the Greenland and Iceland Seas in the late 1980's. Belkin *et al.* (1998) show low salinity in the Iceland Sea in 1989-90, but not as low as at the end of the 1970's, the beginning of the 1980's or at the end of the 1960's. Temperature and negative salinity anomalies in the Labrador Sea at the beginning of the 1990's were as large as in the 1970's and 1980's. Their results show that the iceberg severity index in the North West Atlantic was very large at the beginning of the 1990's. They claim a local origin of this GSA in Labrador Sea, and argue that the sea ice extent anomaly in the Greenland and Iceland Seas was not significant.

Nevertheless, the results from the 41-year run show that the 1989 anomaly in the sea ice export through Fram Strait is due to very thick ice (see Figure 5.6, the anomaly due to the $h'\overline{v}$ term). Consequently, the sea ice extent anomaly may not be so noticeable. The time difference between the peak in sea ice export (1989), and the low in salinity and temperature anomalies in the Labrador Sea (1990-92) is the same order of magnitude as for the GISA of the 1970's. The anomaly of 3000 km^3 in the sea ice export through Fram Stait is the same order as that during the 1967-68 period and therefore is sufficient to create salinity and temperature anomalies in the

Labrador Sea as observed there at the beginning of the 1990's.

The sea ice export anomaly in 1995 obtained from the 41-year run is even larger than those during 1967-68 and 1981-83, and was observed by Vinje *et al.* (1998). This sea ice export anomaly is due to an anomaly in the sea ice velocity (see Figure 5.6, the anomaly due to the $v'\overline{h}$ term). Figure 5.6 corresponds well with Figure 5.7, showing the importance of the northerly wind stress in the sea ice export anomaly. Many studies consider the northerly wind in the Fram Strait region to be the main driving mechanism for the sea ice export. Generally, the northerly wind anomalies and the sea ice export anomalies are significantly correlated for the occurrence of the peaks but not for their magnitude. Alekseev *et al.* (1997) and Smirnov and Smirnov (1998) used statistical data-based models to estimate the sea ice export through Fram Strait relating the pressure gradient in this region to the sea ice export by a linear relation. The years covered by the observations show a very high agreement between the two quantities but they are quite sparse in time. This approach totally neglects the evolution of the sea ice in the Arctic, which is subject to large deformations in the regions of convergence and near the coastlines. These lead to ridging, and create important sea ice thickness anomalies which can be advected along the basin (Tremblay and Mysak, 1998) and hence influence other deformations events in the basin. This now leads us to the next section where the influence of different atmospheric patterns in the Arctic Basin will be explored.

5.3 Sea ice interannual variability in the Arctic Basin

The results in the previous section show the importance of the sea ice thickness in creating anomalies of sea ice export through Fram Strait. Therefore, the evolution of the sea ice cover in the Arctic Basin is very important. Walsh and Chapman

(1990) pointed out that the variability in the index of the pressure difference between southern Greenland and the Arctic-Asian coast corresponds well with the large sea ice export in the 1960's. They concluded that thicker ice (multi-year ice) from the Arctic Basin could be advected into the Fram Strait region and make export larger than it would have been had the sea ice been wind driven only. The results of the previous section (see Figure 5.6) confirm this conclusion. Therefore, we first want to consider ice volume anomalies in the Arctic Basin. Secondly, we wish to determinate how and where they originate, and lastly, we want to find the atmospheric patterns which create them and force their propagation toward Fram Strait.

The sea ice volume and sea ice extent were computed from the model results. A mean sea ice thickness of 3.1 m and a mean sea ice extent of $6.7\text{x}10^6 km^2$ over the 41-year period were obtained. The latter agrees with the result of $6.5\text{x}10^6 km^2$ obtained by Parkinson *et al.* (1987). The computed 3.1-m mean thickness over the Arctic Basin agrees well with the 3-m mean ice thickness estimated by Aagaard and Carmack (1989). Thus, the computed mean ice volume is 2.08 $\text{x}10^4 km^3$. The annual anomalies in sea ice volume for the Arctic Basin are computed for the 41-year period and compared with the sea ice export anomaly through Fram Strait (see Figure 5.8). The two quantities are comparable in magnitude. In addition Figure 5.8 suggests that there seems that the large ice export events are preceded by a large ice volume anomaly ,with the peak ice volume anomalies leading the peak export anomalies by about two years.

In order to analyse the evolution of the Arctic Ocean sea ice volume anomalies, the Arctic Basin is divided into 9 regions (see Figure 5.9): region 1: Beaufort Sea; region 2: Chukchi Sea; region 3: East Siberian Sea; region 4: south central Arctic; region 5: Laptev Sea; region 6: central north Arctic; region 7: north of Greenland and Canadian Archipelago; region 8: north of Fram Strait, and region 9: Kara and Barents Seas).

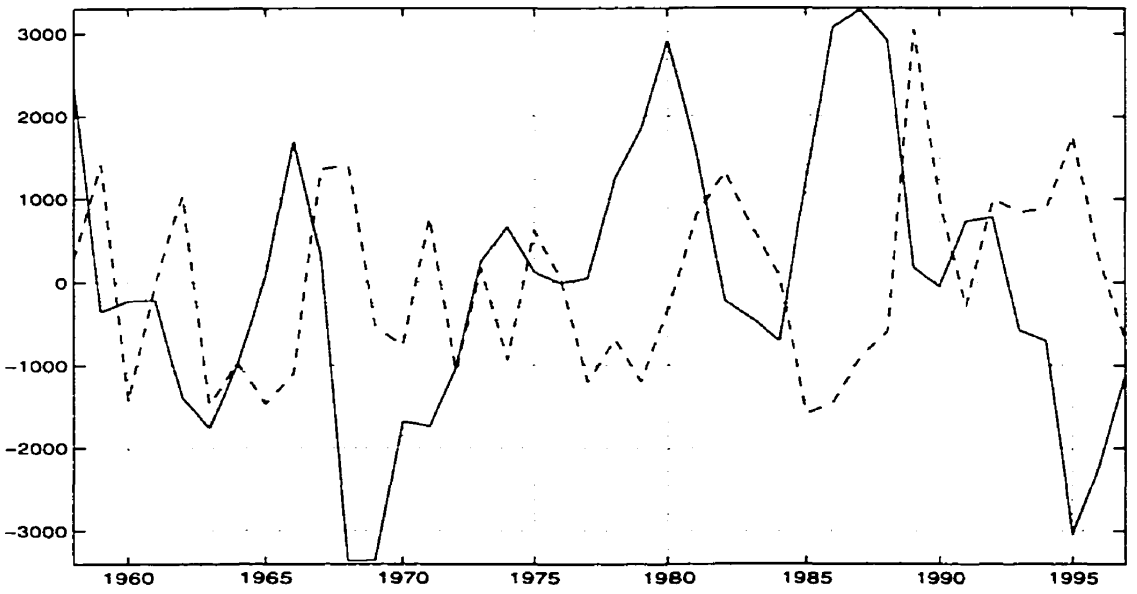

Figure 5.8: Annual mean sea ice volume anomaly in the Arctic Basin (solid line) in km^3 versus sea ice export anomaly through Fram Strait (dashed line) in km^3/yr.

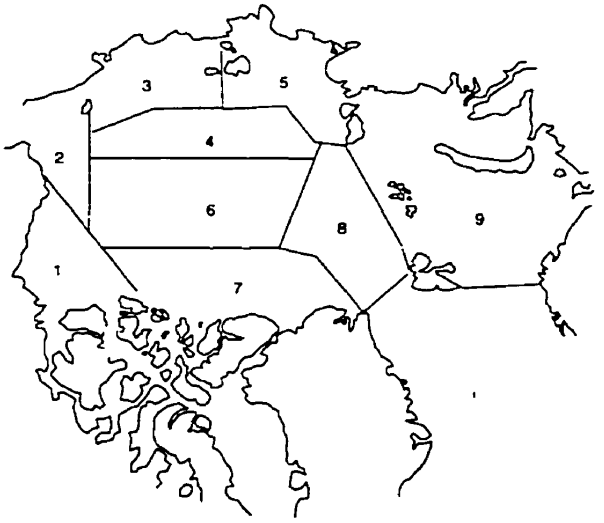

Figure 5.9: The Arctic Basin divided into 9 regions.

The sea ice volume anomaly was then computed for each region (see Figure 5.10). The sea ice volume anomalies in region 9 are not plotted in Figure 5.10 since it was not a significant region for the origin of the sea ice volume anomalies. The region 1 (*i.e.* Beaufort Sea) contributes in 1964, when a sea ice volume anomaly occurs (this agrees with Tremblay and Mysak (1998)), but only a small part is transported through to region 2 (*i.e.*, Chukchi Sea, see Figure 5.10a and b), and then to regions 3 and 4 (Figure 5.10c and d). In 1973 and 1974, an anomaly starts to grow in regions 1 and 2, but a season-by-season analysis of the results (not shown here) showed that this sea ice volume anomaly remained a local anomaly, and disappeared at the end of 1975. A very small sea ice volume anomaly which formed during the summer of 1976 in region 1 seems to have been transported to region 2, and then to region 3.

For increasing volume periods preceding large export periods, the volume anomalies start to form and increase first in regions 3 (*i.e.* East Siberian Sea), where they grow earlier than the basin volume anomalies of 1965-67, 1977-81, and 1985-89. The sea ice volume anomaly then starts to grow in region 4. This is not evident for the first event (1964-66), but it is certainly the case for the two other events. The increase in the ice volume anomaly appears in the central Arctic (region 6). Region 5 (*i.e.*, Laptev Sea) gives only an important contribution to the volume anomaly of 1966 (see Figure 5.10e). The large sea ice volume anomaly which appears during the 1978-81 period (2000 km^3 in the East Siberian Sea) is not transported completely from the region 3 to the regions 4 and 6; it seems to remain a more local feature since only a little more than two-thirds of the anomaly created in region 3 can be found in regions 4 and 6. This is different than in the two other events of 1964-66 and 1985-88, where the same anomaly can be found later in regions 4 and 6.

The ice volume anomalies peak up in regions 7 and 8 (see Figures 5.10 g and h), and after which they start to decrease in regions 4 and 6. Again, for the 1978-81 period not all the sea ice anomaly is transported from the last two regions to regions

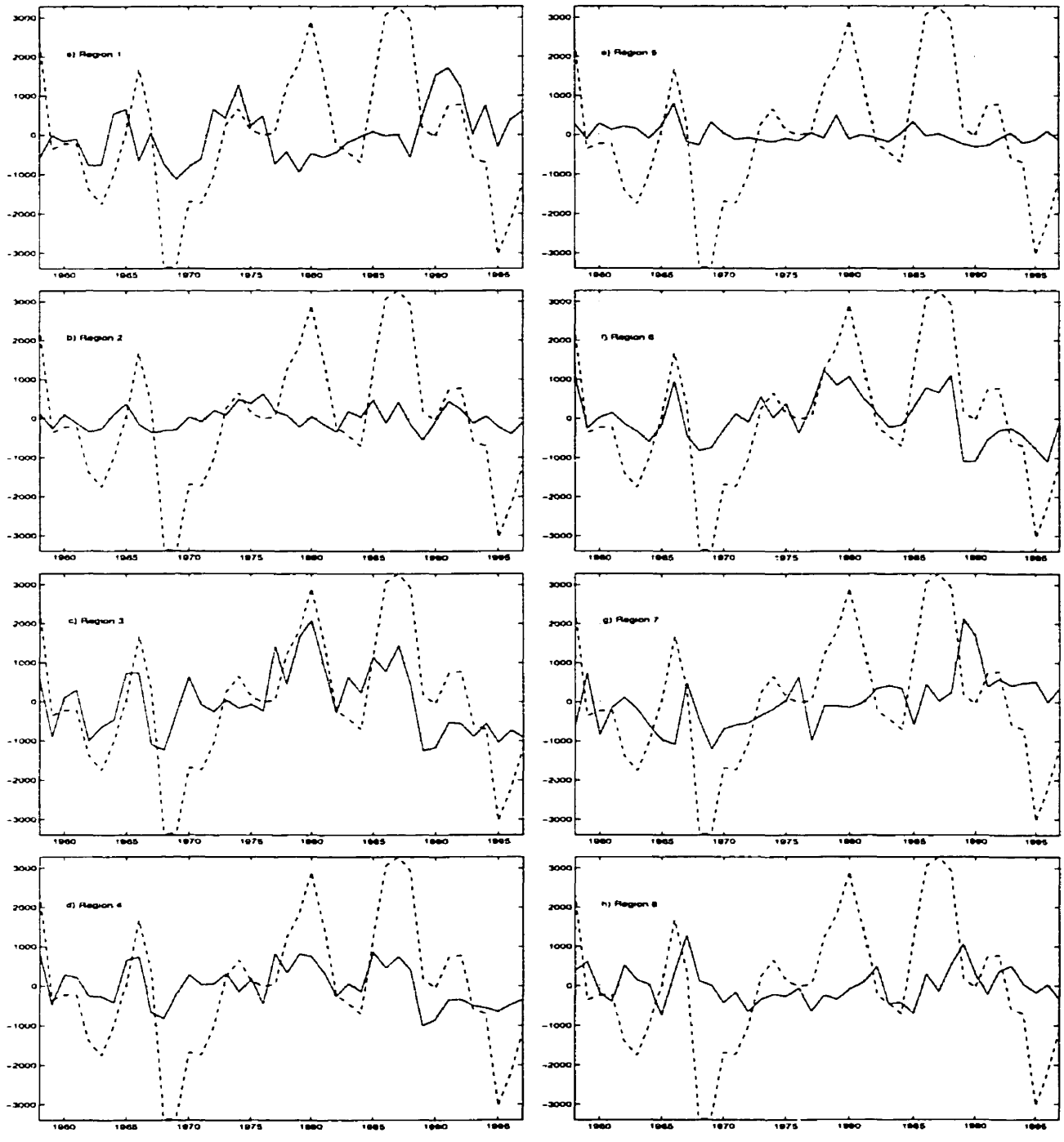

Figure 5.10: Sea ice volume anomalies in km^3 for eight of the regions (solid lines) and for the whole Arctic Basin (dashed line): 1-Beaufort Sea (a), 2-Chukchi Sea (b), 3-East Siberian Sea (c), 4-south central Arctic (d), 5-Laptev Sea (e), 6-north central Arctic (f), 7-north of Greenland and Canadian Archipelago (g), and 8-north of Fram Strait (h).

7 and 8 before beeing exported through Fram Strait. The sea ice volume anomaly in region 8 is smaller than the export for the periods where the large sea ice export is due to an anomaly in the velocity (see Figures 5.6, and 5.10h). Since the circulation increases in this region, there is no important accumulation of sea ice during the 1981-83 period and especially during the 1994-95 period. For the years of large export due to an anomaly in thickness, the sea ice volume anomaly is visible (*i.e.*, in 1967 and 1989). For the large sea ice export 1967-68 period, when the anomaly was due to the change in sea ice velocity peaks ($v'\overline{h}$ term), there was no more accumulation of sea ice and the sea ice volume anomaly decreased rapidly even though the export still had a large value.

In the region 7, north of the Canadian Archipelago and north of Greenland, the sea ice volume shows two large anomalies, during 1967 and 1989, corresponding to two years of large sea ice export through Fram Strait. Serreze *et al.* (1992), following on from the Walsh and Chapman (1990) results, examined the atmospheric pressure gradient between Ellesmere Island and the North Pole. They concluded that the multi-year sea ice comes from along the northern coasts of Greenland and Ellesmere Island where the sea ice is very thick (up to 7 or 8-m) due to packing along this coastline. Walsh and Chapman (1990) showed that the pressure difference between southern Greenland and the Arctic-Asian coast has the same variability as the sea ice export through Fram Strait and also leads the latter.

The atmospheric pressure difference between Ellesmere Island and the North Pole used by Serreze *et al.* (1992) had a large value from 1964 to 1970, but it did not show the same variability as the sea ice export through Fram Strait. Since this variability exists in the pressure difference between southern Greenland and the Arctic-Asian coast, the variability should be expected to exist in the pressure difference between North Pole and the Arctic-Asian coast. Thus, the anomaly in the sea ice export should be transported via the Transpolar Drift Stream, and the hypothesis proposed

by Serreze *et al.* (1992) would not be correct. Since the results in the sea ice volume anomaly in region 7 (see Figure 5.10g) show a positive anomaly in 1967 (of 400 km^3), this region was divided into 2 bands, one adjacent to the coast and another to the north of the first band in order to verify whether this anomaly would contribute to the sea ice export through Fram Strait. It was then found that the anomaly was effectively transported to north of Fram Strait from the band that was farther away from the coast. Therefore, it can only be attributed to an anomaly transported from region 6. For the peak in 1989, the results show that the sea ice volume anomaly comes effectively from the coast and does not appear in the northernmost of the 2 bands; it goes directly to region 8 before it is exported through Fram Strait. One part of the anomaly was going from the region 7 to region 1 (1990). Therefore, multi-year sea ice formed along the coast of Greenland and Canadian Archipelago can be advected through Fram Strait, but this did not seem to be the case during the 1967-68 period, as proposed by Serreze *et al.* (1992).

This general anticyclonic circulation in the Arctic Basin agrees with the model results obtained by Tremblay and Mysak (1998) who showed that an anomaly formed in the Beaufort Sea could be transported around the basin with the same anticyclonic circulation and the same timescale (around 3 years). For example, this anticyclonic circulation in the Arctic Basin of positive sea ice volume anomalies was mainly formed in the East Siberian Sea region and can be seen on Figure ?? for the 1984-89 period.

These results can be further explained by looking at the sea level pressure patterns from the NCEP Reanalysis Data set and the sea ice velocity fields obtained from the 41-year run for the following ice volume periods: 1964-66, 1978-80, 1985-88, 1991-1993 (see Figures 5.12a, b, and c, 5.13a, b, and c, 5.14a, b, and c, 5.15a, b, and c,), and the large export periods 1967-68, 1981-83, 1989, and 1994-95 (see Figures 5.12d, e, and f, 5.13d, e, and f, 5.14d, e, and f, 5.15d, e, and f)

The mean sea level pressure (SLP) was computed for these periods (figure a or d).

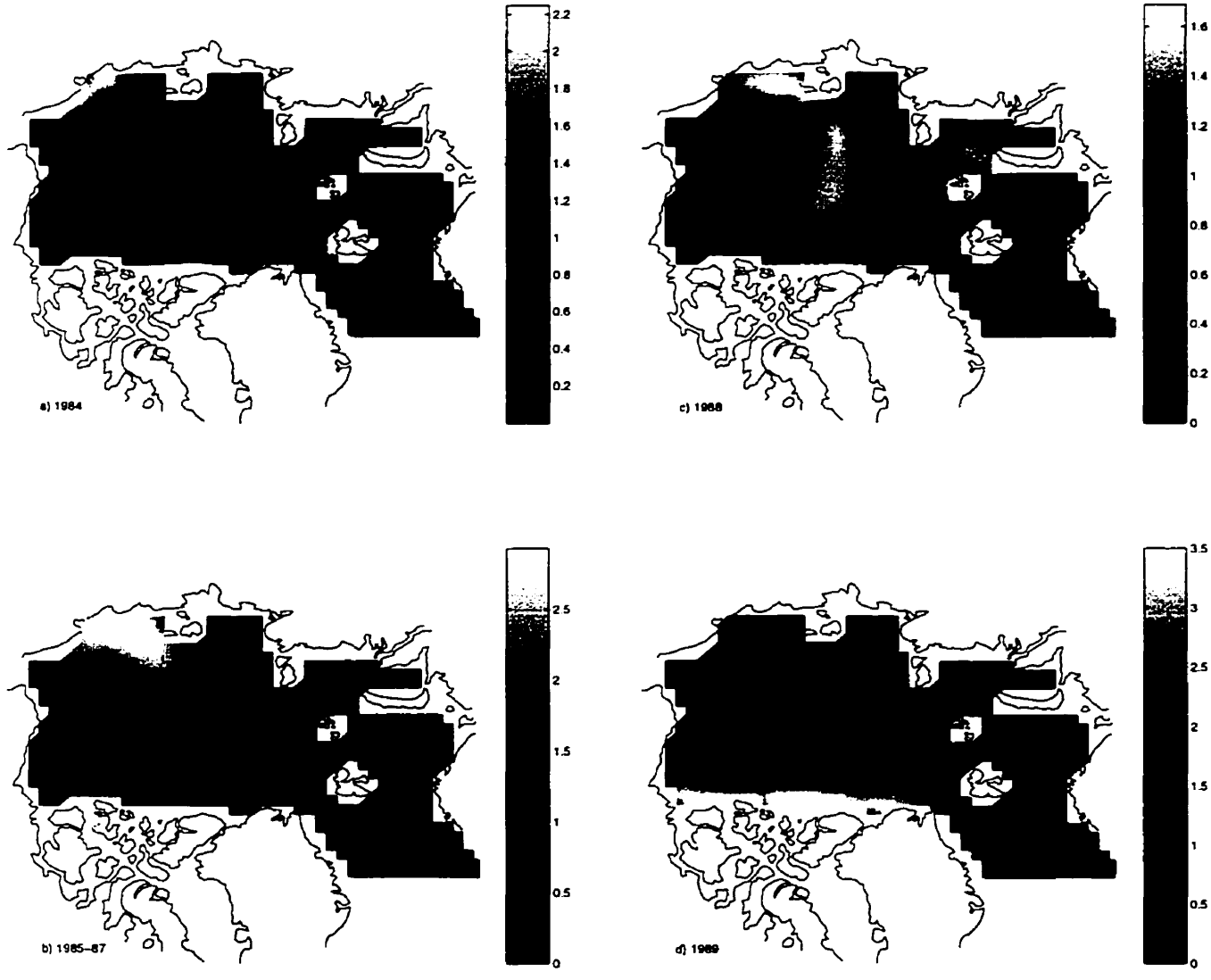

Figure 5.11: Positive sea ice volume anomalies for the 6-year period 1984-89 with the main increasing ice volume during the 1985-87 period. Thickness scales to the right of each figure are in meters, and each colorbar has a different scale.

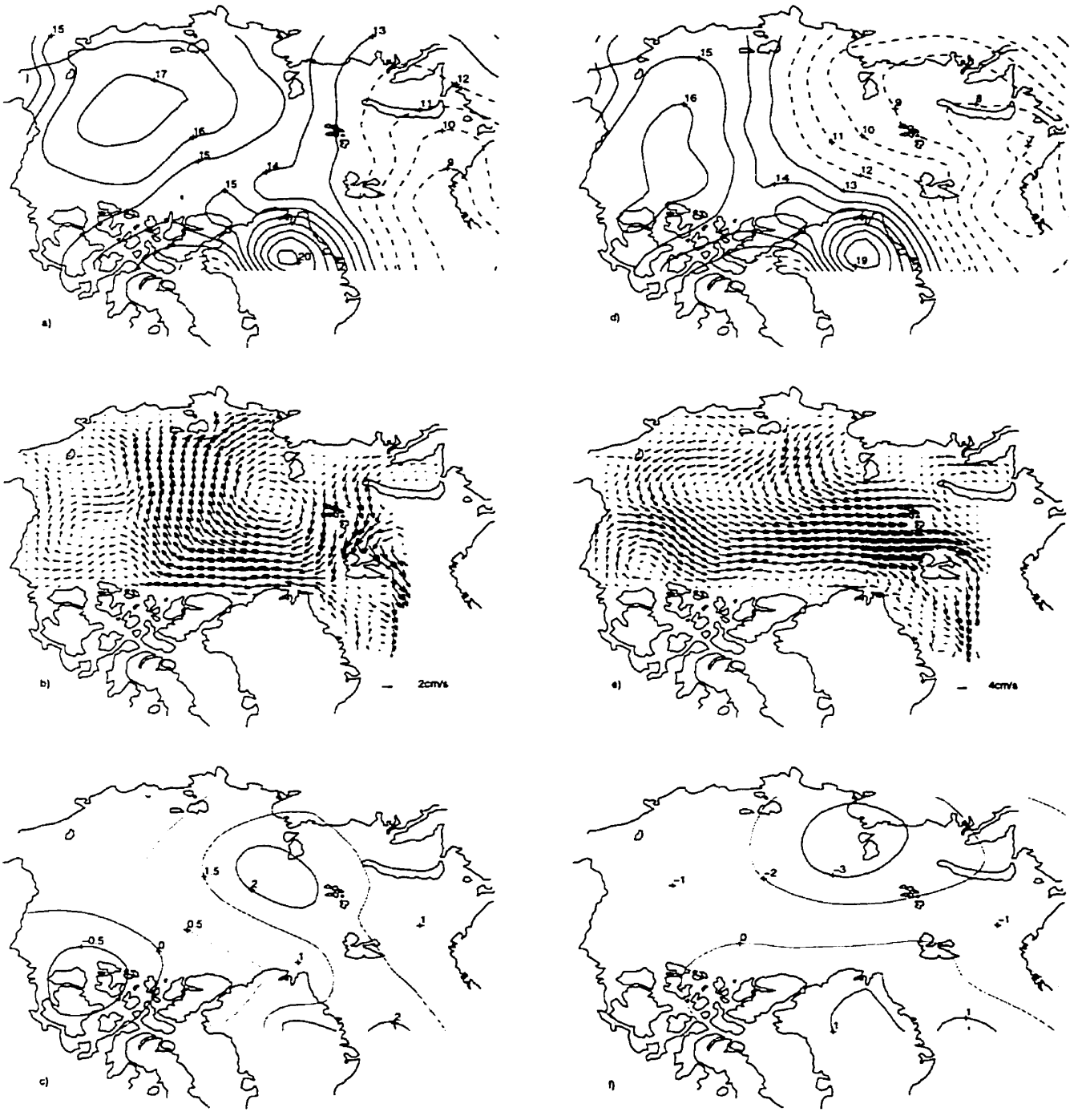

Figure 5.12: Mean sea level pressure in mb (relative to 1000 mb), anomaly in the mean sea ice velocity field, and anomaly in the mean sea level pressure field in mb for the 1964-66 period (a, b, and c), and 1967-68 period (d, e, and f).

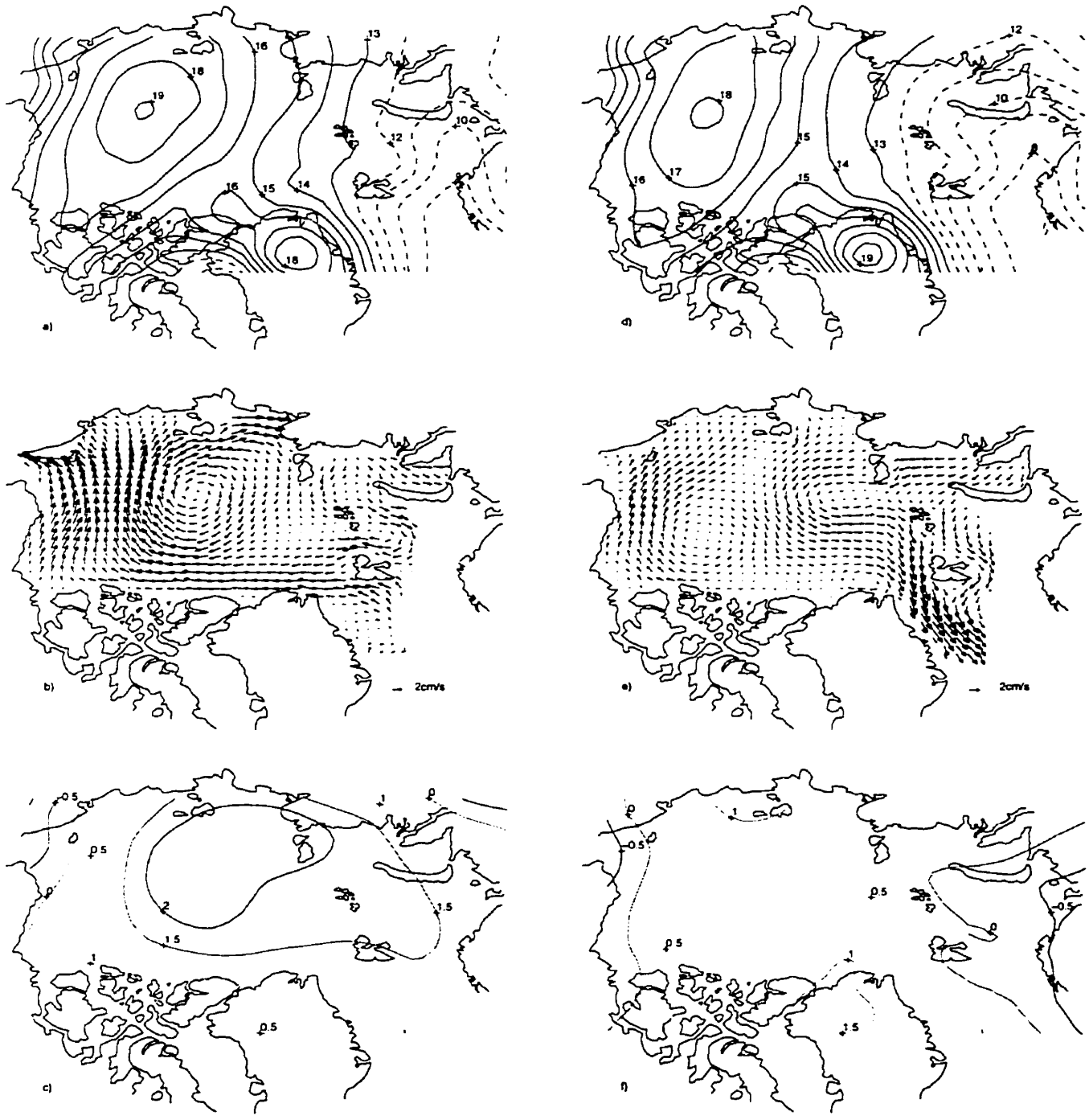

Figure 5.13: Mean sea level pressure in mb (relative to 1000 mb), anomaly in the mean sea ice velocity field, and anomaly in the mean sea level pressure field in mb for the 1978-80 period(a, b, and c), and 1981-83 period (d, e, and f).

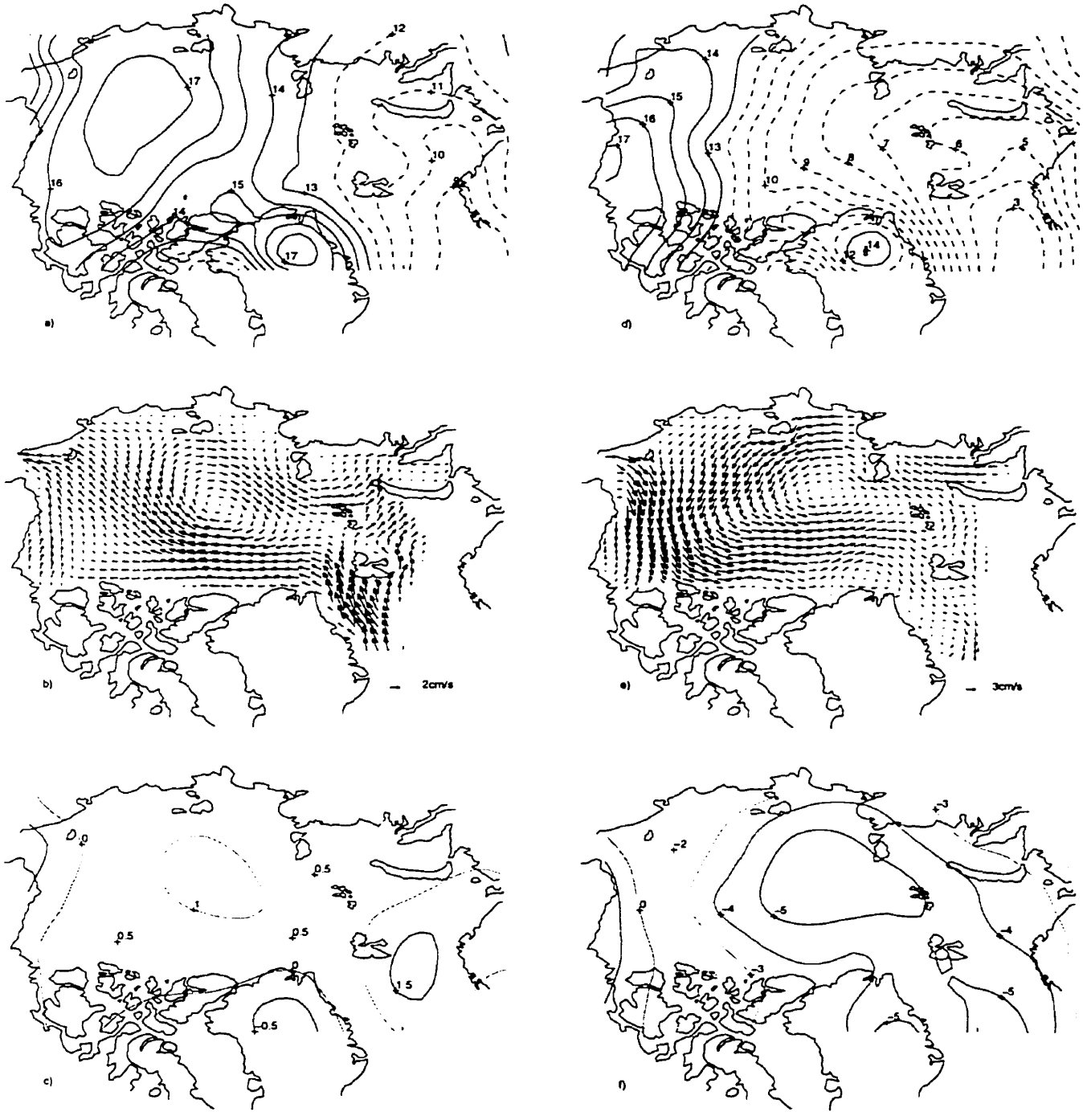

Figure 5.14: Mean sea level pressure in mb (relative to 1000 mb), anomaly in the mean sea ice velocity field, and anomaly in the mean sea level pressure field in mb for the 1985-88 period (a, b, and c), and the year 1989 (d, e, and f).

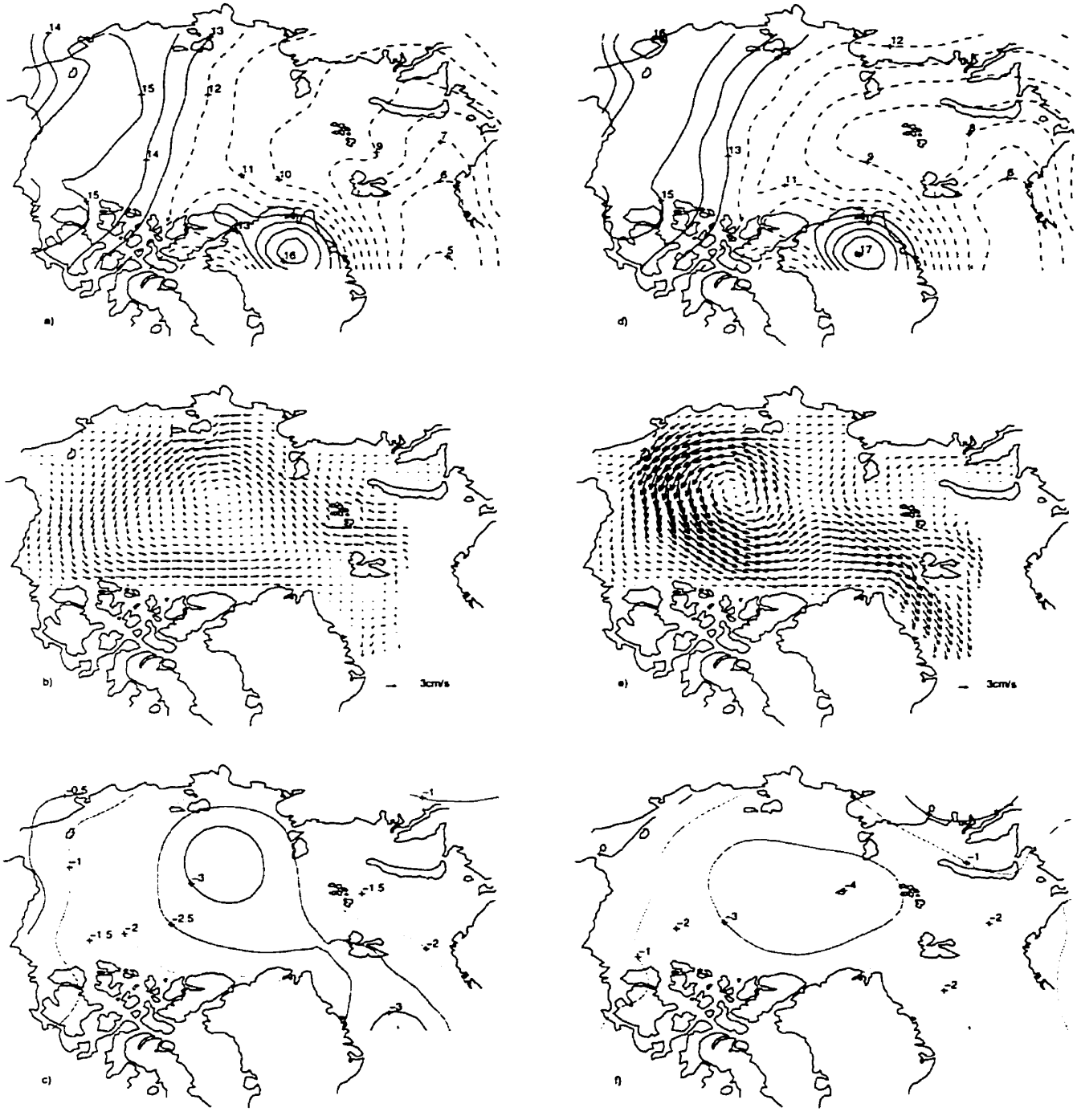

Figure 5.15: Mean sea level pressure in mb (rerelative to 1000 mb), anomaly in the mean sea ice velocity field, and anomaly in the mean sea level pressure field in mb for the 1990-93 period (a, b, and c), and 1994-95 period (d, e, and f).

For the same periods the mean sea ice velocity fields were computed and the climatological sea ice velocity field from the 41-year run (see Figure 4.11) was subtracted from these mean sea ice velocity fields to yield anomaly fields (figure b or e). The anomaly in the mean SLP fields (figure c or f) was also computed for these periods by subtracting the mean of the 41-year run from the mean SLP over the corresponding period.

The anomalies in the sea ice velocity field for the 1967-68 period (see Figure 5.12e) show that the export of the thick ice from along the coast of Greenland and the Canadian Archipelago was not possible because ice circulation along the coast was extremely weak. This is due to the presence of the pocket-shape made by the 1015-mb isobar north of Ellesmere Island. The situation is different in 1989, with a stronger circulation along the coast, which allows the ice to leave the coast and then go to the Fram Strait region (see Figure 5.14e).

Anomalies in the sea ice velocity field show that for three of the four periods of increasing sea ice volume in the Arctic Basin (1964-66, 1978-80, and 1985-88) the ice circulation tends to pack the ice along the East Siberian coast more than usual. Since it is in this region that the volume anomalies in the Arctic Basin grow, the origin of this increase is the packing of the ice along the coast of East Siberia. It is remarkable that during these periods of volume increase, the high pressure system over the Arctic Basin is centered closer to the Asian continent with isobars showing a geostrophic wind which pushes the ice along the coast. The SLP anomalies show a higher SLP than usual along the East Siberian Coast (positive anomaly); this is in agreement with the previous result of the Arctic high centered to the south near the East Siberian Coast. This agrees well with the results obtained by Gudkovich (1961) who compared the atmospheric pressure distribution to the observed currents in the Arctic Basin (these results are also reported in Proshutinsky and Johnson (1997)). Gudkovich (1961) showed that two types of circulation exist in the Arctic Basin:

the cyclonic circulation corresponding to the climatology (years of large export, see below), and a more anticyclonic circulation, with the Beaufort High closer to the Siberian coast which the author call the Siberian High (northern extension of the Asian High located over Siberia). The Transpolar Drift Stream slows and shifts toward North America, leading to cyclonic sea ice circulation in the East Siberian Sea. Gudkovich reports that at such a time the navigation conditions are favorable in Kara Sea but especially unfavorable with presence of thick ice in the Laptev Sea and East Siberian seas. These atmospheric conditions lead to packing of the sea ice along the coast, as we mentioned before, and make the navigation conditions unfavorable.

Anomalies in the sea ice velocity fields (see parts b and e in Figures 5.12-15) follow the isobars of the SLP anomalies (see parts c and f in Figures 5.12-15) of the forcing fields.

Only during the 1964-66 period is there an accumulation of ice in the Laptev Sea (see Figure 5.10). Sea ice velocity anomalies (see Figure 5.12b) tend to pack more of the ice than usual in this region. The Laptev Sea plays a large role in the Arctic as a source of first-year sea ice; it is a polynya which does not store the sea ice but produces it.

For periods of large sea ice export anomalies, the sea ice velocity fields confirm that the circulation tends to transport more ice from the center of the Arctic Basin (where the volume anomalies are located) to the Fram Strait region. The SLP patterns show a configuration of the isobars which allows a strong Transpolar Drift Stream, *i.e.* isobars going from the Laptev Sea to the Fram Strait region quite directly, with generally a strong lateral gradient. This agrees with the results in the sea ice velocity fields showing a well developed Transpolar Drift Stream for periods of large export(*e.g.*, see sea ice velocity fields for the year 1968, in Figure 5.16). The SLP patterns show also that these periods of large export correspond to an Icelandic Low extending farther than normal into the Arctic Basin, corresponding well with the retreat of the Arctic

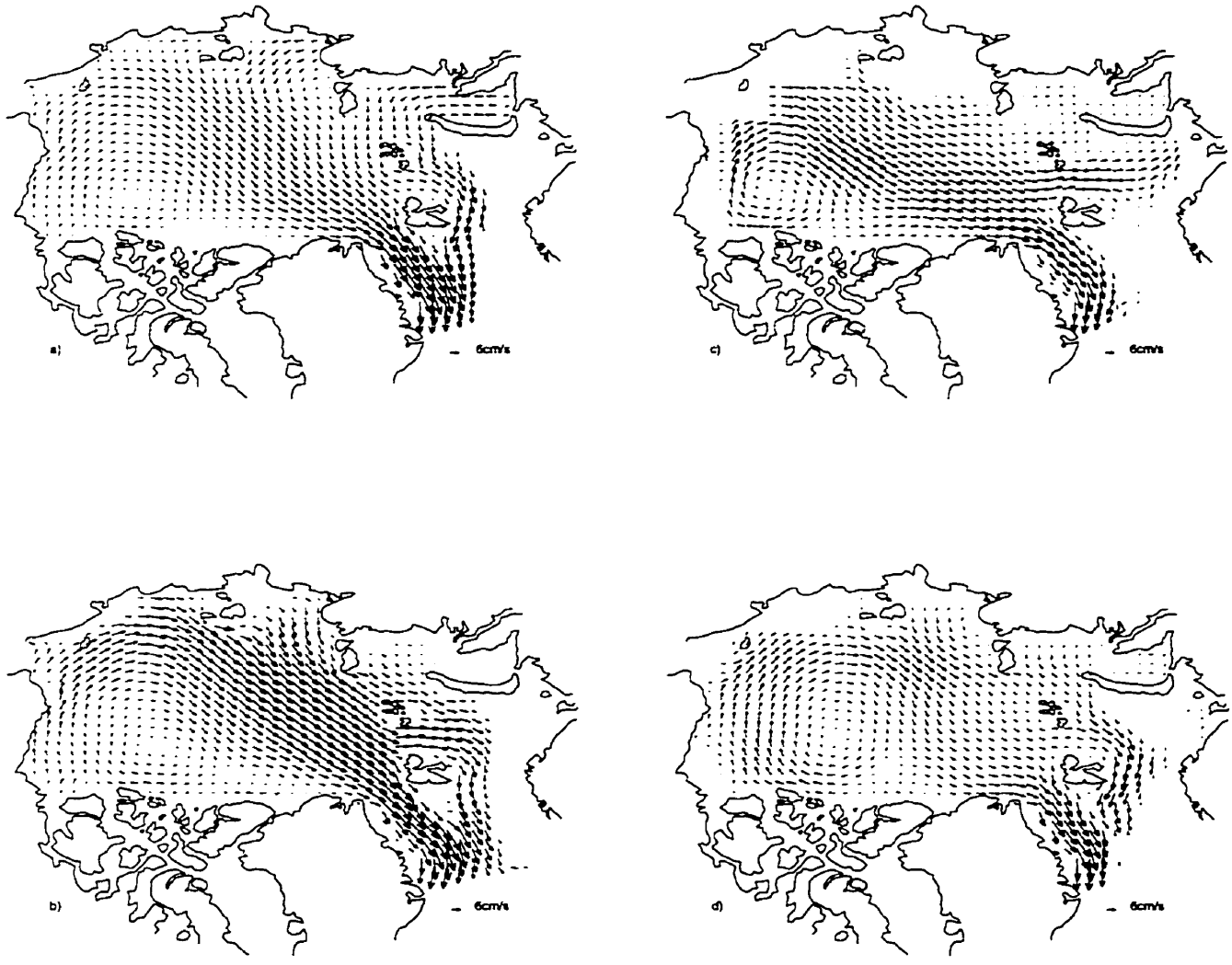

Figure 5.16: Sea ice velocity field for the (a) winter (JFM), (b) spring (MAJ), (c) summer (JAS), and (d) autumn (OND) 1968.

High, to the southern part of the Beaufort Sea. This is confirmed by the negative SLP anomalies or a very weak positive anomaly in the western part of the Arctic Basin.

The results mentioned above indicated that during the 1978-81 period, the ice volume anomaly in the Arctic Basin did not propagate as much as during other periods. The sea ice velocity anomalies (see Figures 5.13b, and e) show that the ice packing along the coast was quite large, and that during the export period (1981-83) this anomaly is persistent in keeping the sea ice in the East Siberian Sea until 1982.

An interesting result is that the large export in 1995 was not preceded by a strong increase of volume in the Arctic Basin (see Figure 5.8). This is the second largest export in the results of the 41-year run, and it is a realistic result since it was observed by Vinje *et al.* (1998). During the 1990-93 period the export is also quite high. The SLP patterns (see Figures 5.15a, and d) show an anomalous situation for the 1990-93 period; the large intrusion of the Icelandic Low in the Arctic stayed that way during a long period (1989-95). During the period 1996-97 the Arctic High is still far east of the Arctic Basin (not shown here), allowing a well developed Transpolar Drift Stream and no sea ice volume formation in the East Siberian Sea.

During the 1989-95 period, sea ice conditions in the East Siberian Sea were lighter than usual as reported by Maslanik *et al.* (1996). The authors related these conditions to the large increase in the number of intense winter cyclone events in the late 1980's in North Atlantic and North Pacific, as reported by Lambert (1996). During the 1989-95 period, the Arctic Oscillation (AO) index (Thomson and Wallace, 1998) was higher than usual, a situation corresponding to a deeper Polar Vortex, which means a more cyclonic atmospheric circulation over the Arctic Basin (more cyclone events). McPhee *et al.* (1998) related the observed anomalous thin sea ice and freshening near the center of the Beaufort Gyre during the SHEBA (Surface Heat Budget of the Arctic Ocean) experiment to the deepening of the Polar Vortex and a more cyclonic

circulation in the Arctic Basin. These results correlate well with our results showing a negative anomaly in the SLP pattern for the 1989-98 period, corresponding to a more cyclonic atmospheric circulation over the basin, which drives a more cyclonic sea ice circulation and also implies no large sea ice volume formation in the East Siberian Sea.

Thomson and Wallace (1998) compared their AO index with the surface air temperature over land in Siberia and showed that the two quantities are highly correlated and that the high AO index after the late 1980's corresponds to warmer surface air temperatures over land in Siberia. The authors explain these warm surface air temperature conditions by the aforementioned large extent of the Icelandic Low in the Arctic during the 1989-98 period, which would have brought warmer than usual air over Siberia.

The anomalous situation for the 1989-98 period could be related to the results obtained by Lambert (1996) which showed a very large increase in the number of intense winter cyclone events in northern North Atlantic and Pacific since the late 1980's. The winter northerly wind stress in the Fram Strait region computed from the NCEP Reanalysis data set shows a large increase in the late 1980's (not shown here).

An interesting quantity which characterizes the winter atmospheric circulation in the North Atlantic is the North Atlantic Oscillation (NAO) index. The sea ice export through Fram Strait is more clearly correlated to the NAO index after the mid 1970's (see Figure 5.17) when there was an increase of the number of intense winter cyclone events in northern North Atlantic (Lambert, 1996). This would correspond in average to a deeper Icelandic low and would confirm the extended low pressure in the eastern side of the Arctic Basin. It should be noted that the highest correlation between the NAO index and the sea ice export is for the peak in 1989, which is due to an anomaly in sea ice thickness (see Figure 5.6) and not to a large sea ice velocity which would be

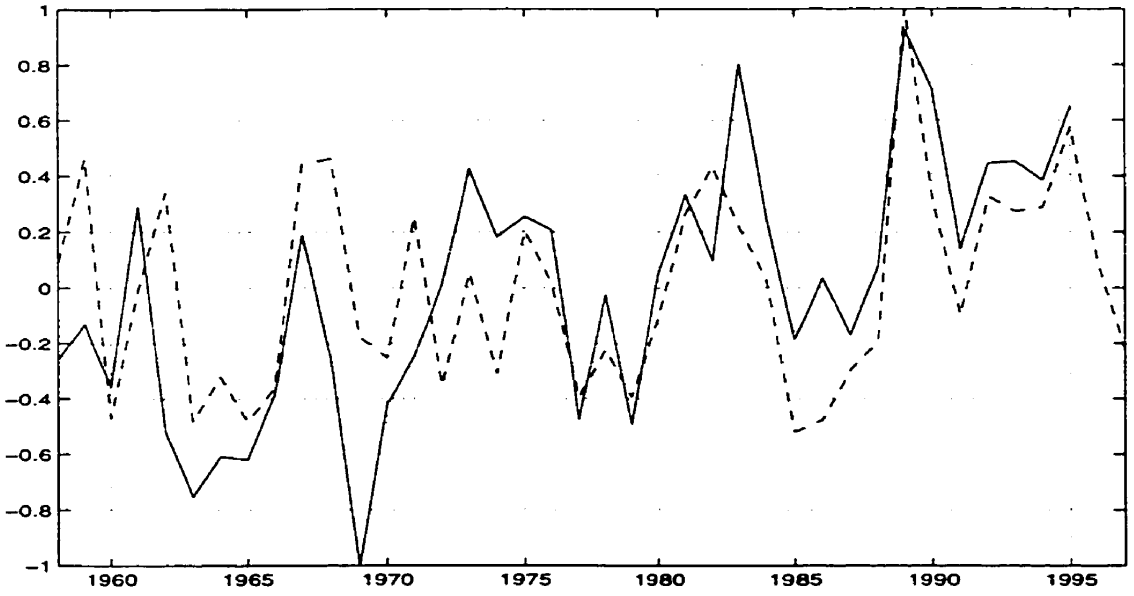

Figure 5.17: Normalized NAO index (solid line) versus normalized sea ice export through Fram Strait (dashed line). (These time series were normalized by the maximumvalues in the series.)

a simple conclusion that could be drawn from the Figure 5.17. Therefore, it is very important to consider the atmospheric state in the Arctic Basin, which is certainly related to the atmospheric states in the North Pacific and North Atlantic, in order to understand the variability in the sea ice cover in the Arctic Basin and the sea ice export associated with the transport of sea ice in the Arctic Basin.

Chapter 6

Conclusions

The interannual variability of the sea ice conditions in the Arctic Basin is simulated for the 41-year period 1958-98 using a thermodynamic-dynamic sea ice model based on granular material rheology. The NCEP Reanalysis data set is used to force the model with climatological monthly-mean surface air temperatures and monthly mean wind stresses. This approach resulted in the the thesis being focussed on the changes in the ice conditions that result from changes in the wind field.

The results from a 20-year spin-up using the NCEP climatology as forcing data and the climatology of the full 41-year run using monthly mean wind stresses are examined and correspond well with available data for sea ice cover. However, the climatology of the 41-year run is closer to the observed climatology than that from the 20-year spin-up run. This shows that the results are more realistic with interannually varying (less smooth) forcing, but the use of monthly mean wind stresses are still smooth the effects of short timescale synoptic events.

First, the year-by-year results for the sea ice export through Fram Strait are compared with other sea ice export simulations covering the 26-year period 1960-85 and with observed values for the 6-year period August 1990 to August 1996. These comparisons suggest that sea ice export anomalies through Fram Strait are realistic.

Secondly, the relation between large sea ice exports through Fram Strait for the periods 1967-68, 1981-83, and 1989 and important climate events such as the GISA of the 1960's and 1970's, the GSA of the 1980's and the probable GSA of the 1990's are examined.

These revealed that the large export during the 1967-68 period can be intepreted as the origin of the GISA of the 1960's and 1970's in the Greenland and Iceland seas, which subsquently resulted in large negative salinity and temperature anomalies in the upper waters of the Labrador Sea at the beginning of the 1970's that later were advected around the North Atlantic subpolar gyre during the 1970's. The GSA of the 1980's is more difficult to explain in terms of prior sea ice export anomalies through Fram Strait. Large export during the 1981-83 period reached its peak too late to be the major cause of this GSA; however, the large export in 1981 could have participated significantly at the early stages of the event. A reasoning based only on a local origin in the Labrador Sea of this event does not seem sufficient to explain the observed temperature and salinity anomalies in the 1980's. Fresh water transport through the Canadian Archipelago could have played an important role, but this feature is not resolved by our model. The probable GSA of the 1990's can be explained by the large sea ice export through Fram Strait in 1989, the largest export of the 41-year period 1958-98. This, however, was not accompanied by a large sea ice extent in the Greenland Sea.

Sea ice export through Fram Strait is decomposed into anomaly terms due to the sea ice velocity and thickness. It is shown that some large sea ice exports through Fram Strait can be explained by either a thickness anomaly (*e.g.*, in 1989) or a sea ice velocity anomaly alone (, *in e.g.* 1995). Other exports, on the other hand, can be explained by anomalies in both quantities. The decomposition shows the importance of the sea ice thickness anomaly in the sea ice export. For example, the large sea ice export through Fram Strait in 1989 is explained by very thick ice formed inside of the

Arctic Basin. This result can explain why there was no particularly large sea ice extent anomaly in Greenland Sea in 1989. Peaks in strength of the northerly wind in the Fram Strait region correspond well with the large sea ice export due to anomaly in the sea ice velocity, for example in 1995. Another interesting result is that the product of the sea ice thickness and velocity anomalies is small and shows that the two quantities are not correlated in the Fram Strait region. Therefore, the two quantities are not directly related in this region. The results underline the importance of the sea ice evolution in the Arctic Basin, and show that the sea ice export through Fram Strait is not simply dependent on wind in the Fram Strait region. Thus, the interannual variability of the sea ice volume anomaly in the Arctic Basin is also investigated.

The sea ice export and volume anomalies show related interannual variabilities. In general, large sea ice exports are preceded by large sea ice volume anomalies in the Arctic Basin. For both quantities there are five regularly spaced extreme events over the 41-year period 1958-98. This would suggest a periodicity of approximately 7-8 years. Proshutinsky and Johnson (1997) showed the existence of two different regimes in the wind-driven sea ice circulation in the Arctic Basin, each persisting for 5-7 years, suggesting a periodicity of 10-14 years, which is somewhat larger than the present case. Two complex EOF studies, Mysak and Venegas (1998) and Venegas and Mysak (1998) pointed out that the Arctic sea ice extent exhibits a clockwise propagating signal whose period ranges from 8 to 13 years.

In general, most of sea ice volume anomalies are transported through the Arctic Basin before being exported through Fram Strait. In order to analyze the origin and the evolution of the sea ice volume anomalies, the Arctic Basin is divided into 9 regions. The results show that the sea ice volume anomalies are generally formed in the East Siberian Sea and propagate toward the center of the Arctic Basin in an anticyclonic (clockwise) direction, which is consistent with Mysak and Venegas (1998). They are then advected directly to the Fram Strait region and along the

north Greenland coast, and are exported through Fram Strait. The hypothesis of multi-year sea ice from the north Greenland coast could be supported by the results of the 1985-89 period; however even in this case, thick ice is mainly formed in the East Siberian Sea.

To understand the physical origins of the sea ice volume anomalies and their propagation, the anomalies in the sea ice velocity fields and the SLP patterns for the sea ice volume anomaly formation periods and the large export periods are investigated. Sea ice velocity anomalies show that during the sea ice volume formation periods, the sea ice is packed more than usual along the East Siberian coast. The SLP patterns show that during these periods the Beaufort High is closer to the East Siberian coast. SLP anomaly patterns confirm that the SLP is higher than usual in the centre of the basin near the Asian coasts, which allows winds to pack the sea ice in the East Siberian Sea.

During the large export periods, the anomalies in the sea ice velocity fields show that the circulation tends to advect more sea ice than usual from the center of the Arctic Basin to the Fram Strait region, and hence transports the sea ice volume anomalies out of the Arctic Basin through Fram Strait. The SLP patterns show that at this time the Beaufort High is relocated closer to the Beaufort Sea with the Icelandic Low extending far into the Arctic Basin, which provides for a well developed Transpolar Drift Stream. Again, the SLP anomalies confirm these results.

During the 1990-98 period, the atmospheric conditions do not allow for the packing of the ice in the East Siberian Sea. The Beaufort High is still centered near the Beaufort Sea and the Icelandic Low is still extending far into the Arctic Basin. In this case, large exports during this period should be due to an anomaly in sea ice velocity. This is consistent with the sea ice export anomalies results and their decomposition into sea ice thickness and velocity anomalies, which show that the export is still quite large in the 1990's and that the large export in 1995 (the second largest of the

41-year period) is due not to an anomaly in sea ice thickness but to an anomaly in sea ice velocity. This recent period corresponds to a period of very strong increase in the number of intense winter cyclones in the northern North Atlantic and Pacific (Lambert, 1996). In addition, Smith (1990) shows the increase in the length of the melt season of perennial Arctic sea ice over the same period, and Maslanik *et al.* (1996) relate these anomalous atmospheric conditions to recent decreases in Arctic summer ice cover.

These results makes it even more important to consider the sea ice transport through regions like the Canadian Archipelago Straits. In the recent decrease of sea ice cover and stronger atmospheric circulations, which could be due to global warming, more sea ice could be transported through the Canadian Archipelago Straits into the northern North Atlantic and may thus modify deep water formation in the Labrador Sea. However, the work done by Anderson *et al.* (1998), points out the possible importance of the Arctic Basin as a region of deep water formation which could drive the global conveyor belt. In both cases this makes it very important to understand the mechanisms involved in ice production in the Arctic Basin and surrounding seas since these region are very sensitive to the change in atmospheric conditions and can feed back on them. A comparison of the sea ice export anomalies with the NAO index does not show an evident correlation for the whole 41 years; but the two time series seem to correlate well after 1975, and especially after the late 1980's. At this time there was an increase in the number of intense winter cyclone events in northern North Atlantic and Pacific. Atmospheric conditions in the Arctic Basin are certainly related to those in the North Atlantic and the North Pacific via the Arctic Oscillation (Thomson and Wallace, 1998); but atmospheric conditions in the Arctic Basin should be considered closely, and the Arctic Basin should be considered as a particular region in order to understand the influence of the atmospheric conditions on the sea ice cover,especially those conditions associated with global warming.

Appendix A

Physical parameters and constants used in the simulation

Table A.1: Physical parameters and constants used in the simulation

Variable	symbol	value
Ice albedo	α_i	0.67
Land albedo	α_l	0.80
Ocean albedo	α_o	0.17
Atmospheric emissivity	ϵ_a	0.88
Ice emissivity	ϵ_i	0.97
Land emissivity	ϵ_l	0.90
Ocean emissivity	ϵ_o	0.96
Planetary emissivity	ϵ_p	0.50
Internal angle of friction	ϕ	30 degrees
Maximum ice viscosity	η_m	1×10^{12} kg/m/s
Air density	ρ_a	1.3 kg/m^3
Ice density	ρ_i	900 kg/m^3
Water density	ρ_w	10^3 kg/m^3
Stefan-Boltzmann constant	σ	5.67×10^{-8} W/(m^{2}K^4)
Air and water turning angle	θ_a, θ_w	25 degrees
Ice strength parameter	C	20
Air drag coefficient	C_{da}	$3 \times 1.2 \times 10^{-3}$
Water drag coefficient	C_{dw}	$4.5 \times 5.5 \times 10^{-3}$
Latent heat transfer coefficient	C_{lat}	1×10^{-3}
Specific heat of air	C_{pa}	$1 \times 10^3 J/(KgK)$
Specific heat of water	C_{pw}	$4 \times 10^3 J/(kgK)$
Sensible heat coefficient	C_{sens}	1×10^{-3}
Atmospheric scale height	H_a	8.4×10^3 m
Land thickness	H_l	6 m
Ocean mixed layer depth	H_o	100 m
Atmospheric diffusion coefficient	K_a	5×10^{12} m^2/ s
Ice thermal conductivity	K_i	2 W/(m K)
Land thermal conductivity	K_l	2 W/(m K)
Ocean diffusion coefficient	K_o	1×10^{10} m^2/s
Latent heat of evaporation	L_e	2.50×10^6 J / kg
Latent heat of fusion	L_f	3.34×10^5 J / kg
Latent heat of sublimation	L_s	2.83×10^6 J / kg

Table A.1: Physical parameters and constants used in the simulation, (continued)

Variable	symbol	value
Ice strength in compression	P_{max}	27×10^3 N/m^2
Sea level pressure	P_s	101.3×10^3 Pa
Solar radiation constant	Q_0	1340 W/m^2
Ocean freezing point	T_{fp}	-1.8 C°
Fresh water freezing point	T_{fi}	0 C°
Land base temperature	T_{lb}	6.0 C°
Coriolis parameter	f	1.5×10^{-4} s^{-1}
Gravitational acceleration	g	9.81 m/s^2

Bibliography

AAGAARD, K. AND CARMACK, E. C. (1989). The role of sea ice and other fresh water in the Arctic circulation. *Journal of Geophysical Research*, 94:14485–14498.

AAGAARD, K. AND GREISMAN, P. (1975). Toward new mass and heat budgets for the Arctic Ocean. *Journal of Geophysical Research*, 80:3,821–3,827.

ALEKSEEV, G. V., MYAKOSHIN, O. I., AND SMIRNOV, N. P. (1997). Variability of the ice transport through the Fram Strait. *Meteorologiya i Gidrologiya*, 9:37–41.

ANDERSON, L. G., JONES, E. P., AND RUDELS, B. (1998). Evaluation of the Arctic Ocean as a significant driver of the northern contribution to the global conveyor belt. *Journal of Geophysical Research (submitted)*.

BARNETT, D. G. (1980). A long-range ice forcasting method for north coast of Alaska. In PRITCHARD, R. S., editor, *Sea Ice Processes and Models*, pages 360–372. University of Washinton Press.

BELKIN, I. M., LEVITUS, S., AND ANTONOV, J. (1998). Great Salinity Anomalies in the North Atlantic. *Progress in Oceanography*, 41:1–68.

BOURKE, R. H. AND GARRETT, R. P. (1987). Sea ice thickness distribution in the Arctic Ocean. *Cold Regions Science and Technology*, 13:259–280.

CAMPBELL, W. J. (1965). The wind-driven circulation of ice and water in the polar ocean. *Journal of Geophysical Research*, 70:3279–3301.

CHAPMAN, W. L. AND WALSH, J. E. (1993). Recent variations of sea-ice and air temperature in high latitudes. *Bulletin American Meteorological Society*, 74:33–47.

DICKSON, R. R., MEINCKE, J., MALMBERG, S.-A., AND LEE, A. J. (1988). The "Great Salinity Anomaly" in the northern North Atlantic 1968-1982. *Progress in Oceanography.*, 20:103–151.

ECKARDT, M., GALLAS, J., AND TONN, W. (1992). Sea ice distribution in the Greenland and Barents seas based on satellite information for the period 1966-89. *International Journal Of Remote Sensing*, 13:23–35.

FLATO, G. M. AND HIBLER, III, W. D. (1992). Modeling pack ice as a cavitating fluid. *Journal of Physical Oceanography*, 22:626–651.

FLEMING, G. H. AND SEMTNER, A. J. (1991). A numerical study of interannual ocean forcing on Arctic sea ice. *Journal of Geophysical Research*, 96:4589–4603.

GRAY, J. M. N. T. AND MORLAND, L. W. (1994). A two-dimensional model for the dynamics of sea ice. *Philosophical Transactions of the Royal Society of London*, 347:219–290.

GUDKOVICH, Z. M. (1961). Relation of the ice drift in the Arctic Basin to ice conditions in Soviet Arctic seas (in Russian). *Tr. Okeanogr. Kom. Akad. Nauk SSSR*, 11:14–21.

HÄKKINEN, S. (1993). An Arctic source for the Great Salinity Anomaly: A simulation of the Arctic ice-ocean system for 1955-1975. *Journal of Geophysical Research*, 98:16,397–16,410.

HÄKKINEN, S. (1995). Simulated interannual variability of the Greenland Sea deep water formation and its connection to surface forcing. *Journal of Geophysical Research*, 100:4,761–4,770.

HIBLER, III, W. D. (1979). A dynamic thermodynamic sea ice model. *Journal of Physical Oceanography*, 9:815–846.

HIBLER, III, W. D. AND WALSH, J. E. (1982). On modeling seasonal and interannual fluctuations of Arctic sea ice. *Journal of Physical Oceanography*, 12:1514–1523.

KASSENS, H., DMITRENKO, I., RACHOLD, V., THIEDE, J., AND TIMOKHOV, L. (1997). Russian and German scientists explore the Arctic's Laptev Sea and its climate system. *EOS, Transactions, American Geophysical Union*, 79:317–323.

LAMBERT, S. J. (1996). Intense extratropical northern hemisphere winter cyclone events:1899-1991. *Journal Of Geophysical Research*, 101:21319–21325.

LAZIER, J. R. N. (1980). Oceanographic conditions and at Ocean Weather Ship Bravo 1964-1974. *Atmosphere-Ocean*, 18.

LEVITUS, S. (1994). World ocean atlas 1994, cd-rom data sets.

MASLANIK, J. A. AND DUNN, J. (1997). On the role of sea-ice transport in modifying Arctic responses to global climate change. *Annals of Glaciology*, 25:102–106.

MASLANIK, J. A., SERREZE, M. C., AND BARRY, R. G. (1996). Recent decreases in Arctic summer ice cover and linklages to atmospheric ciculation anomalies. *Geophysical Research Letters*, 23:1677–1680.

MAURITZEN, C. AND HÄKKINEN, S. (1997). Influence of sea ice on the thermohaline circulation in the North Atlantic Ocean. *Geophysical Research Letters*, 24:3257–3260.

MAYKUT, G. A. AND UNTERSTEINER, N. (1971). Some results from a time-dependent thermodynamic model of sea ice. *Journal of Geophysical Research*, 76:1550–1575.

MCLAREN, A. S., SERREZE, M. C., AND BARRY, R. G. (1987). Seasonal variations of sea ice motion in the Canada basin and their implications. *Geophysical Research Letters*, 14:1123–1126.

MCPHEE, M. G. (1975). Ice-ocean momentum transfer for the AIDJEX Ice model. *AIDJEX Bulletin*, 29:93–111.

MCPHEE, M. G. J., STANTON, J. H., MORISON, J. H., AND MARTINSON, D. J. (1998). Freshening of the upper ocean in the Arctic: Is perinnial sea ice disapearing? *Geophysical Research Letters*, 25:1729–1732.

MYSAK, L. A. AND MANAK, D. K. (1989). Arctic Sea-Ice Extent and Anomalies. 1953–1984. *Atmosphere-Ocean*, 27:376–405.

MYSAK, L. A., MANAK, D. K., AND MARSDEN, R. F. (1990). Sea ice anomalies observed in the Greenland and Labrador Seas during 1901-1984 and their relation to interdecadal Arctic climate cycle. *Climate Dynamics*, 5:111–133.

MYSAK, L. A. AND POWER, S. B. (1992). Sea-ice anomalies in the western Arctic and Greenland-Iceland sea and their relation to an interdecadal climate cycle. *Climatological Bulletin*, 26(3):147–176.

MYSAK, L. A. AND VENEGAS, S. A. (1998). Decadal climate in the Arctic: A new feedback loop for atmosphere-ice-ocean interaction. *Geophysical Research Letters*, 25:3607–3610.

PARKINSON, C. L. AND CAVALIERI, D. J. (1989). Arctic sea ice 1973-1987: Seasonal, regional, and interannual variability. *Journal of Geophysical Research*, 94:14,499–14,523.

PARKINSON, C. L. AND WASHINGTON, W. M. (1979). A large-scale numerical model of sea ice. *Journal of Geophysical Research*, 84:311–337.

PROSHUTINSKY, A. Y. AND JOHNSON, M. A. (1997). Two circulation regimes of the wind-driven arctic ocean. *Journal of Geophysical Research*, 102:12,493–12,514.

SEMTNER, A. J. (1976a). A model for the thermodynamic growth of sea ice in numerical investigations of climate. *Journal of Physical Oceanography*, 6:379–389.

SEMTNER, A. J. (1976b). Numerical simulation of the arctic ocean circulation. *Journal of Physical Oceanography*, 6:409–425.

SEMTNER, A. J. (1987). A numerical study of sea ice and ocean circulation in the Arctic. *Journal of Physical Oceanography*, 17:1,077–1,099.

SERREZE, M. C., MASLANIK, J. A., BARRY, R. G., AND DEMARIA, T. L. (1992). Winter atmospheric circulation in the Arctic Basin and possible relationships to the Great Salinity Anomaly in the northern North Atlantic. *Geophysical Research Letters*, 19:923–296.

SMIRNOV, A. N. AND SMIRNOV, N. P. (1998). *Climate change and Biota of the North Atlantic.* Russian State Hydrometeorological University.

SMITH, W. O. (1990). *Polar Oceanography. Part A: Physical Science.* Academic Press.

THOMSON, D. W. J. AND WALLACE, J. M. (1998). The Arctic Oscillation signature in the wintertime geopotential height and temperature fields. *Geophysical Research Letters*, 25:1297–1300.

TREMBLAY, L.-B. AND MYSAK, L. A. (1997). Modelling sea ice as a granular material, including the dilatancy effect. *Journal of Physical Oceanography*, 27:2342–2360.

TREMBLAY, L.-B. AND MYSAK, L. A. (1998). On the origin and evolution of sea-ice anomalies in the Beaufort-Chuckchi Sea. *Climate Dynamics*, 14:451–460.

UNTERSTEINER, N. (1961). On the mass and heat budget of the Arctic sea ice. *Arch., Meteorol., Geophys. Bioklimatol. ser.*, A12:151–182.

VENEGAS, S. A. AND MYSAK, L. A. (1998). Arctic sea ice and atmospheric variability on the decadal time scale. *Climate Dynamics (submitted)*.

VINJE, T. E. AND FINNEKASA, F. (1986). The ice transport through the Fram Strait. *Norsk Polarinstitutt Skrifter*, 186:39pp.

VINJE, T. E., NORDLUND, N., AND KVAMBEKK, A. (1998). Monitoring ice thickness in Fram Strait. *Journal of Geophysical Research (submitted)*.

WALSH, J. E. AND CHAPMAN, W. L. (1990). Arctic contribution to upper-ocean variability in the North Atlantic. *Journal of Climate*, 3:1462–1473.

WALSH, J. E., HIBLER, III, W. D., AND ROSS, B. (1985). Numerical simulation of Northern Hemisphere sea-ice variability. *Journal of Geophysical Research*, 90:4847–4865.

WALSH, J. E. AND JOHNSON, C. M. (1979). An analysis of Arctic sea ice fluctuations, 1953-1977. *Journal of Physical Oceanography*, 9:580–591.